UNIVERSITÀ DEGLI STUDI DI PADOVA
FACOLTÀ DI SCIENZE MM.FF.NN.
DIPARTIMENTO DI FISICA

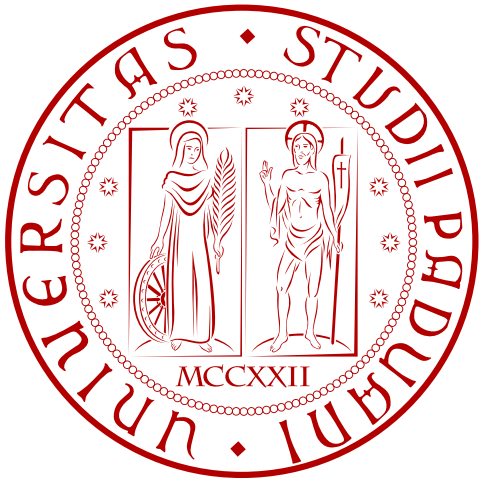

Tesi di Laurea Magistrale in Fisica

Collective Motion in Confining and Non-Differentiable Geometries

Relatore: **Prof. Enzo Orlandini**

Laureando: **Davide Michieletto**

Anno Accademico 2010–2011

A Stefania e alla mia Famiglia,
le parti del mio Tutto.

Contents

The whole is more
than the sum of its parts.

Aristotle

1 Introduction

Collective behaviour has always been one of the most fascinating phenomena since men started to observe Nature. One of the most impressive features is the emerging of collective properties and skills which *do not* belong to the single entity forming the group. This characteristic is particularly attractive and inclined to several practical applications. For these reasons biologists, socio-scientists and zoologists have always been interested in collective behaviours of quadrupeds, birds, fish and insects [1, 2, 3, 4]. These are the most immediate and direct observable examples of species which show collective motion without a leader. On the other hand, in the last century, the biological community started to investigate organisms at even smaller scales. They discovered remarkable collective behaviours and emerging coherent structures in bacteria, cells and metastasis [5, 6, 7] which make these phenomena even more attractive and interesting. Remarkably, the same complex structures are shown by organisms living at very different length scales such as actin molecules and herds.

All these examples have a common property: the elementary units forming the group are classified as "active" or "self-propelled" units, i.e. entities that have the ability to transform, through different ways, the food filling the environment in internal energy and ultimately in motion [8]. Non-living or artificial objects can also be designed as active matter: for instance Chaté *et al.* observed collective behaviours in systems made by polar disks sitting over a vibrating surface [9].

More specifically, the key features shown by these kind of systems are clustering, apolar or polar order and order-disorder transition. Quite surprisingly they are very similar to the collective behaviours occurring in those "pas-

sive" systems, such as spins systems or liquid crystals, deeply understood and well described in Statistical Mechanics.

However, active systems, being formed by self-propelled units, are naturally out-of equilibrium systems, which show novel features like giant density fluctuations and their understanding turns out to be a severe challenge for theoreticians.
For all these reasons statistical physicists began to be interested on the study of these kinds of systems because they offer a practical and popular topic for the in-depth knowledge already held by physicists. Indeed, an analogous physical approach used to describe liquid crystals and spins systems when applied to "active" biological systems, like those made of bacteria and cells, brought many qualitative and quantitative results to biological community and shed new light on the statistical properties of non-equilibrium systems [8, 11]. For these reasons, statistical physicists had, and have currently, the concrete possibility to go further with the study of very interesting features, like non-equilibrium phase transitions, coarsening dynamics, collective response phenomena and giant density fluctuations shown by these "simple" and "easily" reproducible experimentally cases. At the same time, the biologists can take advantage of the results provided by physicists through the understanding of what actually happens in these complex systems and how to describe and predict their peculiar behaviours.

Another important aspect that one has to face in investigating active systems is that self-propelled units often live and move in restricted or crowded environments which, as a first approximation, can be described as narrow and irregular channels. In biology, for instance, micro-organisms like bacteria often move inside human vessels and cytoskeletal motors like kinesin carry proteins and mitochondria to and from neuron cells through microtubule. Moreover, the improvements of nano-scale objects production, like nano-channels and nano-slits, have made possible the design of experiments in which the response of active systems (both natural and artificial) subject to different confinements may be investigated.
For these reasons, in this work we are going to investigate the collective motion of self-propelled particles moving inside narrow and irregular channels. In designing the model and fixing its main parameters we will be inspired by bacterial suspensions inside human vessels although many of the results we will obtain can be often referred to a generic active system.

With this respect, many kind of bacteria, like *E. coli*, adopt, for biochemical reasons, the "run and tumble" behaviour which makes the bacteria to perform a persistent random walks inside the environment. As a consequence, if we consider a system made of *E. Coli* as a mere ensemble of random walkers, we expect it to reach a steady distribution with an homogeneous

density. On the contrary, previous experiments [12] state firmly that geometrical constrains and obstacles lead the system to a completely different density steady distribution even against the Gibbs principle.
Hence, the questions we are going to address and endeavour to answer are: How the bulk collective motions are affected by geometrical constraints? How is it possible to "manipulate" an ensemble of "self-propelled" units by using a given confining geometry? Which new features are brought by the introduction of geometrical irregularities in the confinement? And how we can use them to maximize the coherence in the collective motion of the system?

In order to try to answer to these questions in the first part of this thesis we will report only a brief review regarding the studies (theoretical and experimental) on self-propelled particles bulk features, while the main part will focus on the study of confinement effects and of self-propelled particle-surface interaction on the collective motion. Below is reported a short summary of the chapters in which the thesis is organized:

- **Chapter 2**: A brief review on the Vicsek and Chaté works [10, 13] will be given and many of the numerical results presented in these papers are here reproduced as a stringent test on the correctness of my own code in the unconstrained case (no confinement). The theoretical part is reported as in the works while the data and the plots are obtained using my own code. The results agree with the Vicsek and Chaté ones.

- **Chapter 3**: The excluded volume interaction is here added to the original Vicsek model. The simulations are then performed in the still unconstrained case by using periodic boundary conditions. The effects on the order parameter, order parameter fluctuations, density distribution and spatial correlation are studied. From now on all the models considered will take into account self-propelled particles with excluded volume interactions.

- **Chapter 4**: Confining environments are here considered. We investigate how the constraint affects the order parameter and the order parameter fluctuations. Particular attention is given to the density distribution as a function of the noise and the ratio between system size and particle radius. Several comparisons with periodic boundary conditions are also reported. One of the main results of this chapter, and of the entire work, is shown in sec. 4.3: giant density fluctuations are observed even in confined active systems and found to be related

to the size of the constrained direction.

- **Chapter 5**: Implementation of phenomenologically inspired boundary conditions at the walls. The principal aim here is to design suitable boundary conditions that better reproduce the constrained condition under which bacterial system moves. In particular we will study in details the several collective behaviours that may be induced by the different boundary conditions in strongly confined systems.

- **Chapter 6**: Introduction of "non-differentiable", i.e. irregular, constraints. The simulations are performed using again my own code, parallelized using a mix of OpenMP and MPI, and through the methods reported in sec. 1.1. In particular in this chapter are considered environments which present wedges or bottlenecks. The boundary condition used is the most close to real one, according to [12]. The residence time and the local order parameter are attentively investigated. The introduction of a chemotaxis term and of asymmetric constrains are also briefly studied. The particular case in which a funnel is located in the middle of the system, as experimentally done in [12], is simulated in appendix A.

- **Chapter 7**: I report the main conclusions and some suggestions regarding future works on this topic with the aim to obtain solider and more relevant results especially on the phenomena described in Chapter 6.

1.1 Method

In this thesis the most part of the simulations are performed using a 2D box with specified boundary conditions and with N particles randomly distributed and oriented at the beginning of the process. The data are obtained by averaging the observables the last $5-10\cdot10^3$ time steps and over at least 5 different initial conditions except where specified. The implementation of the excluded volume in chapter 3 is introduced by rejecting all those movements which would create an overlapping of the 2D-volume of two particles within the system. The "walls" and the particle behaviours at the walls in chapters 4 and 5 are implemented through simple conditions at the boundaries. In particular, the "bouncing back" behaviour is reproduced by reflecting the direction of the particles as does the common elastic collision rule. The "stop" condition is taken into account by stopping the motion but letting the direction unchanged while the "slip" condition involves a forced

sliding and reorientation along the wall. Since we are going to work with self-propelled round particles, the first two conditions are quite reasonable, especially if one has in mind the artificial self-propelled particles suggested by the Sheffield researchers. On the other hand, in [12] is firmly proved that the behaviour undertaken by bacteria at the walls is the latter. For this reason in the last chapter (6) only the "slip" boundary condition is considered. For simplicity the collision with the walls is detected when the center of mass of the round particles hits the surfaces; this means that the effective size of the system is the linear size plus the radius of a round particle. The chemotaxis effect in chapter 6 is considered by adding to the usual Vicsek update rule a constant vector pointing to the source of food at each time step.
All the simulations regarding the last part of chap. 6 were performed on Hector, the HPC facility located in Edinburgh. The code has been parallelized by myself for the occasion using a mix of MPI and OpenMP. More detailed information are inside the specified chapters. Some of videos related to specific arguments are uploaded and accessible on my web site http://spiro.fisica.unipd.it/~dmichiel/.

2
Vicsek Model

Contents

In the past decades there has been many attempts to model "flocking" (i.e. collective) behaviour, performed from communities of physicists, biologists and computer graphics specialists.
Perhaps the first model of flocking was introduced by Reynolds in 1987. His system was a collection of "boids", i.e. bird-like particles, subjected to three types of interaction: avoidance of collision, trying to adapting direction to the average one of the neighbours and trying to stay close to the center of mass of the flock. However, his work was only qualitative and "aesthetic"[†].
In order to obtain some quantitative results, in 1995 Vicsek introduced and studied a "naive" model of flocking using the statistical physics approach.
Vicsek's work [10] has immediately found large success and many followers who have been interested on it until nowadays [15, 18, 19, 20, 21].
In the Vicsek model, the activity of the objects is considered making the

[†]For further information see the web site http://www.red3d.com/cwr/boids/

point-like particles move off-lattice at constant speed v_0. Each particle is labelled at each time-step t with its position $\boldsymbol{x}(t)$ and its direction $\vartheta(t) = \Theta(\boldsymbol{v}(t))$, where the function Θ gives the angle between $\boldsymbol{v}(t)$ and a selected direction (horizontal coordinate axis).
The interaction is chosen such that at each time step every particle adjusts its direction of motion to the average one of its neighbours, up to some noise term accounting for the randomness of the system.
As we have already mentioned before, the absolute value of the velocity of each particle is v_0 even after the interaction. As a consequence, this model does not preserve the momentum. Actually, it does not preserve neither the Galilean invariance. Indeed, if we consider a moving reference frame, the absolute velocity of the particles are no longer v_0 as determined by the model.
The random term reproduces the stochastic perturbation affecting the motion of flocking organisms and it is taken into account adding a random angle to the average direction. We will see later that it is not the only way to consider the effects of random perturbation on the direction of motion.
This particular choice reflects the perturbations acting on the decisional mechanism through which each particle updates its velocity. We can call it "angular" (or "intrinsic" [18]) noise. Thus the updating rule is

$$\vartheta_i(t+1) = Arg\left[\sum_{\langle i,j\rangle} e^{\iota\vartheta_j(t)}\right] + \eta\xi_i(t) \tag{2.1}$$

where $\sum_{\langle i,j\rangle}$ is the sum over the particles inside a circle with radius R and with center in $\boldsymbol{x}_i(t)$, η is the noise amplitude ($\eta \in [0,1]$) and $\xi_i(t)$ is a δ-correlated white noise uniformly distributed with $\xi_i(t) \in [-\pi, \pi]$.

An other way to consider stochastic perturbation in the Vicsek model is the so called "vectorial" [13] (or "extrinsic" [18]) noise.
For first, Chàte and Grègiore [13] argued that random errors can be made when a particle estimates the directions of its flock-mates, for example because a noisy environment instead of commit an error when adapt its direction to the average one.
In this respect one has to consider the following updating rule

$$\vartheta_i(t+1) = Arg\left[\sum_{\langle i,j\rangle} e^{\iota\vartheta_j(t)} + \eta n_i(t) e^{\iota\xi_i(t)}\right] \tag{2.2}$$

Where $n_i(t)$ is the number of neighbours of i-th particle at time t.
It is worth to notice that considering vectorial noise instead of angular one is not a pure formality at all. If one use the vectorial noise he makes the locally ordered regions subject to weaker noise than the disordered ones,

indeed in this case also the noise is "averaged".

As already said, the models which tried to describe collective motions were originally inspired by the observation of collective behaviours of flocks of birds, school of fish, swarms of insects and so on. It is useful to have in mind these examples in order to compare the theoretical model with the real world.

2.1 Vicsek Model as Langevin Process Approximation

At first sight the update rules (2.1) and (2.2) seem to be mere tools to reproduce qualitatively the flocking of many interacting objects. On the contrary we are going to point out that those update rules are based on the usual Langevin equations, provided that the friction coefficient is suitable to the case of self-propelled particles as we do in the following deduction. Let us start with the general Langevin equations ($m = 1$):

$$\frac{d\boldsymbol{v}(t)}{dt} = -\gamma(\boldsymbol{v})\ \boldsymbol{v}(t) + \boldsymbol{F}(t) + d\boldsymbol{W}(t) \tag{2.3}$$

$$\frac{d\boldsymbol{x}(t)}{dt} = \boldsymbol{v}(t) \tag{2.4}$$

where $\boldsymbol{F}(t)$ is an external force, $d\boldsymbol{W}(t)$ is the stochastic term (Wiener) and friction term $\gamma(\boldsymbol{v})$. This one is chosen in order to consider the activity of the particles

$$\gamma(\boldsymbol{v}) = \gamma_0 \left(\frac{\boldsymbol{v}^2}{\boldsymbol{v}_0^2} - 1 \right) \tag{2.5}$$

with γ_0 the usual friction coefficient. Indeed this term "pumps" the velocity $|\boldsymbol{v}|$ toward the value v_0, which is reached after an initial transient.
What is important to notice is that

$$\gamma(\boldsymbol{v}) = \gamma(|\boldsymbol{v}|). \tag{2.6}$$

This assumption is quite reasonable and intuitive, indeed it makes sense the assumption that the friction does not affect the direction of the particles. The assumptions we are going to do on the other terms are not so granted, but they lead to the equations provided in the original Vicsek model. Let us assume that the external force $\boldsymbol{F}(t)$ and the stochastic term $d\boldsymbol{W}(t)$ do

not affect the absolute value of the velocity, so one can write:

$$\boldsymbol{F}(t;|\boldsymbol{v}|,\vartheta) = \boldsymbol{F}(t;\vartheta)$$
$$d\boldsymbol{W}(t;|\boldsymbol{v}|,\vartheta) = d\boldsymbol{W}(t;\vartheta).$$

Actually, in the original Vicsek formulation the stochastic term does not neither depend on the direction of the particle but for our purpose these assumptions are enough. At this point is clear that one can rewrite the equation (2.3) as two differential equations; one on the absolute value of the velocity and the other on the direction ϑ.

$$\frac{d\,|\boldsymbol{v}(t)|}{dt} = -\gamma(|\boldsymbol{v}|)\,|\boldsymbol{v}(t)| \tag{2.7}$$
$$\frac{d\vartheta(t)}{dt} = F(t;\vartheta) + dW(t;\vartheta) \tag{2.8}$$
$$\tag{2.9}$$

and for time large enough

$$\frac{d\,|\boldsymbol{v}(t)|}{dt} = 0\ ,\ |\boldsymbol{v}| = v_0. \tag{2.10}$$

Finally one can write the velocity of each particle as follows

$$\boldsymbol{v}(t) = |\boldsymbol{v}(t)|\, e^{\iota\vartheta(t)} = v_0 e^{\iota\vartheta(t)} \tag{2.11}$$

i.e. a vector pointing to the direction $\vartheta(t)$ with norm v_0.
Since that we have to consider the finite step time in order to perform numerical simulations, the evolution equation (2.4) becomes

$$\boldsymbol{x}_i(t+\Delta t) = \boldsymbol{x}_i(t) + \boldsymbol{v}_i(t)\Delta t \tag{2.12}$$

with $\boldsymbol{v}_i(t)$ controlled by eq. (2.8) and (2.10) with the suitable terms for $F(t)$ and $dW(t)$. It can indeed reproduce the equations (2.1) or (2.2) depending on the choice of the stochastic term.

2.2 Algorithm

In this chapter we are going to do a brief review on the main Vicsek [10], Baglietto and Albano [15] works on this topic and to perform independent simulations in order to check the results provided by my own code. The simulations are not large scale simulations, thus we are going to compare them only with the qualitative numerical results provided in the earliest

works mentioned above. Indeed, since that many quantitative works have been already done on the Vicsek model (for example see [22, 27]), our aim is not to provide quantitative and solid results regarding this topic but to test the validity of our algorithm in order to have a solid base from which we can start to work on the real goals of this thesis.

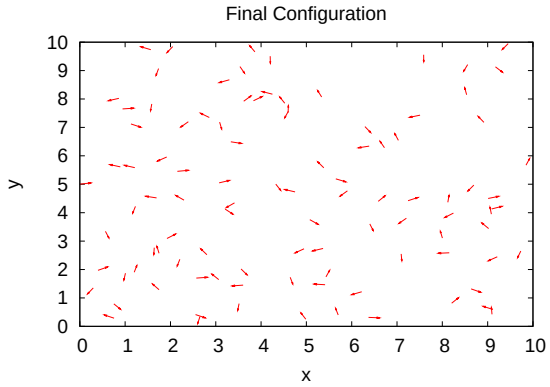

(a) Value of the noise amplitude: $\eta = 0.9$

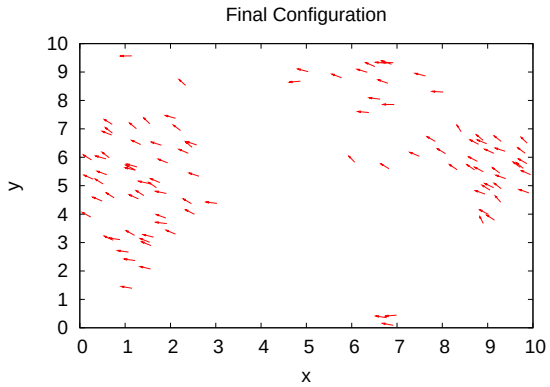

(b) Value of the noise amplitude: $\eta = 0.2$

Figure 2.1: Snapshot of a late time configuration of point-like particles subjected to the angular noise specified below the plots. The system has linear size $L = 10$ and $N = 100$ particles (arrows point to the last direction of particles).

The initial set up is made of N particles randomly distributed and oriented inside a box with linear size L. The boundary conditions are fixed as in the original Vicsek model, i.e. we assume periodic boundary conditions. Thus the particles can move over the surface of a 3-dimensional torus. The time step is fixed to $\Delta t = 1$ as the interactions radius $R = 1$. At every time step each particle "looks" for neighbours inside R, if it has not flock-mates, it considers its own direction as the averaged direction. In other words, unless the noise is null, a particle cannot move straightly even if isolated.

As already said, the particles are point-like, i.e. they have not an excluded volume. Examples of typical configuration are shown for the model based on angular noise in figures 2.1a and 2.1b for high and low values of the noise, respectively. It is worth to notice the coherent moving structures arisen for low noise value.

2.3 Observables

In order to obtain some quantitative results, and inspired by the statistical physics ansatz, we are going to define and measure the (instantaneous) order parameter:

$$\phi(t) \equiv \frac{1}{Nv_0} \left| \sum_{i=1}^{N} \boldsymbol{v}_i(t) \right| . \tag{2.13}$$

In a passive system such as a ferromagnetic one $\boldsymbol{v}$(t) would correspond to the single spin orientation while $\phi(t)$ to the average magnetization at the time step t. Figures 2.2 and 2.3 show the trend of the averaged order parameter $\phi \equiv \langle \phi(t) \rangle$ against the noise amplitude η for angular and vectorial noise respectively. The average has been performed over the configurations as explained in section 1.1. The curves are obtained varying properly the system linear size L and the number of particles N in order to simulate a thermodynamic limit (the number density $\rho \equiv N/L^2$ is kept constant).

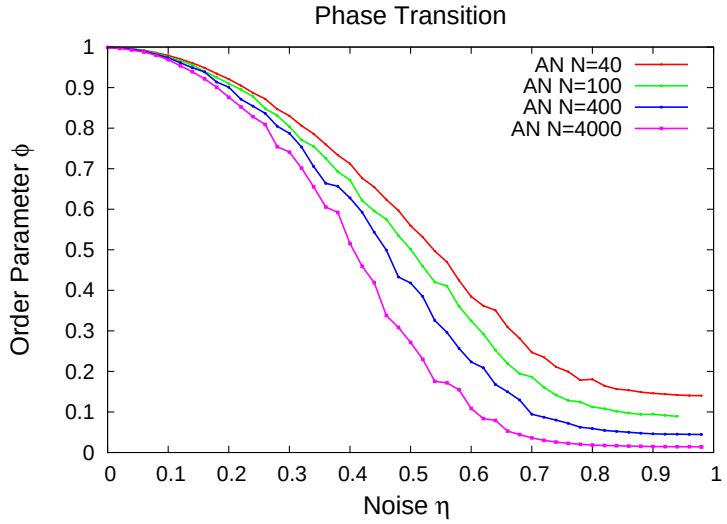

Figure 2.2: Plot of the order parameter ϕ versus *angular* noise amplitude. The curves correspond to different values of number of particles in systems with the same density $\rho = 4$ (N=40, L=3.1; N=100, L=5; N=400, L=10; N=4000, L=31.6).

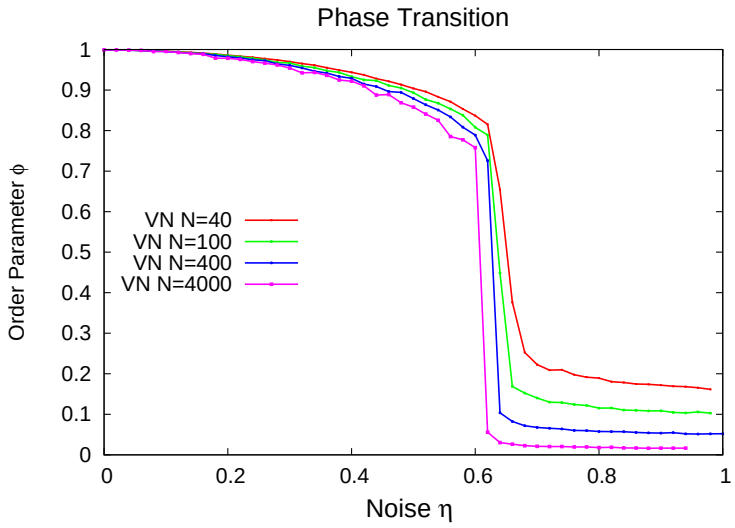

Figure 2.3: Plot of the order parameter ϕ versus *vectorial* noise amplitude. The curves correspond to different values of number of particles in systems with the same density $\rho = 4$ (N=40, L=3.1; N=100, L=5; N=400, L=10; N=4000, L=31.6).

The first imperative consideration to point out is that the system shows a crossover from a disordered state to an ordered one. In other words, under the suitable noise conditions, the system "chooses" a particular direction and breaks the initial rotational symmetry. As a consequence, while the initial total momentum is null (the particles are randomly oriented), the system reaches a state in which it is non-null.

In these plots one can also observe the shift of the curves towards smaller values of the noise for increasing values of the system linear size. This feature strongly suggests that the crossover from the disordered to the ordered state occurs also in the thermodynamic limit and so we can assume that the Vicsek model is able to reproduce a phase transition. Since the Vicsek model describes non-equilibrium systems, the phase transition showed above is called "kinetic", on the contrary, passive (equilibrium) systems show "static" phase transitions.

Another consideration we can do is that the crossover is continuous (2.2) for systems subjected to angular noise while discontinuous (2.3) for systems subjected to vectorial noise. Actually, the classification of the transition shown by the Vicsek model in the two cases was debated for a long period. In the last decade have been done many works focused on large-scale simulations with the aim to identify the type of the Vicsek model phase transition (see [15, 22, 23, 24, 26, 25]). In particular, the shift of the curve in fig. 2.2

raised a lot of questions regarding the effects of the system "finite size" on the type of crossover, and if it could be different when the thermodynamic limit is considered. In [15] large scale simulations and *ad hoc* tricks (as rotating reference frames) are performed by the authors in order to remove as far as possible the system finite-size effects. In the same work is firmly stated that the phase transition ($N \to \infty, L \to \infty$) is effectively a second type phase transition (continuous) when the system is subjected to angular noise, while it is a first type phase transition (discontinuous) when subjected to vectorial noise.

It is worth to notice that the onset of the ordered phase is not granted at all, indeed the correspondent "passive" model (the XY model for spin systems) can not show any phase transition in $d = 2$, as stated by Mermin-Wagner theorem [31]. This characteristic of the model is absolutely non-trivial. Indeed even nowadays the thought that a flock can be seen as a *phase* of a system made of birds or a school as a phase of a system made of fish is quite weird.

2.3.1 Scaling Properties

Quite remarkably, the order parameter behaviour plotted in fig. 2.2 and 2.3 is very similar to the order parameter trends of some equilibrium systems close to their critical point, such as, for instance, the magnetization for ferromagnetic systems; even though in standard equilibrium systems the critical behaviour is usually expressed as function of the temperature and density, in this case we write ϕ as function of the noise η and the density ρ. As a consequence, one could identify the noise introduced "by hand" in eq. (2.1) and (2.2) with a sort of system temperature.
Actually, if we consider, for instance, a real system made of bacteria in an aqueous bath, one could argue that the temperature of the system involves strong consequences on the bacteria behaviour. One can moreover guess that in this case the Vicsek noise could be even proportional to the temperature of the bath. This argument suggests that the analogy noise-temperature is not so wrong, and will be useful to keep in mind.
For these reasons and in analogy with the scaling law for the magnetization, one can guess a scaling law also for the order parameter ϕ:

$$\phi(\eta, \rho; L) = \begin{cases} \left(\dfrac{\eta_c(\rho; L) - \eta}{\eta_c(\rho; L)} \right)^{\beta} & \text{for } \eta < \eta_c(\rho; L) \\ 0 & \text{for } \eta > \eta_c(\rho; L) \end{cases} \tag{2.14}$$

where β is the critical exponent and $\eta_c(\rho; L)$ is, like the critical temperature in ferromagnetic systems, the effective critical value of the noise for finite-size system at density ρ. It is worth to notice that the dependence of η_c from

the system linear size L is quite relevant and has to be taken into account, as we have already seen in fig. 2.2 and 2.3.
The original work [10] provides a rough evaluation of $\eta_c(\rho) \equiv \eta_c(\rho;\infty)$. The numerical value is determined through the maximization of the scaling region and through the check of its increasing for $N, L \to \infty$. Subsequently, large-scale simulations in [20] have provided solider numerical estimation of $\eta_c(\rho;\infty)$ giving the finite-size scaling law

$$\eta_c(\rho, L) - \eta_c(\rho, \infty) \sim L^{-1/2}. \tag{2.15}$$

On the contrary, the estimation of $\eta_c(\rho; L)$ is easier and it is provided from Gaussian fit (see fig. 2.4) of the order parameter fluctuations, defined as follows

$$\chi = \mathrm{Var}(\phi) L^2 \qquad \mathrm{Var}(\phi) \equiv \langle \phi(t)^2 \rangle - \langle \phi(t) \rangle^2. \tag{2.16}$$

where, as usually, $\langle \dots \rangle$ represents the average over the configurations.

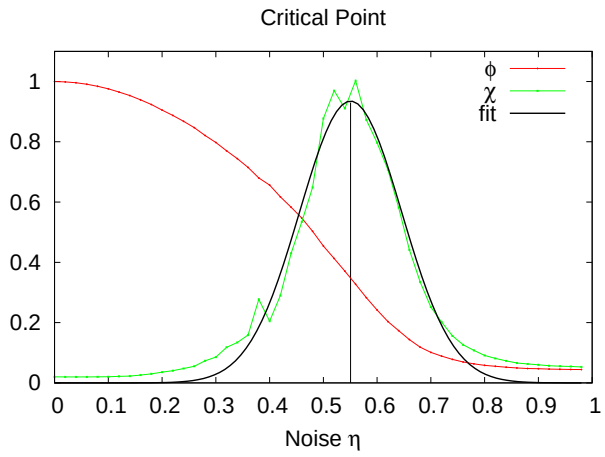

Figure 2.4: Example of order parameter and order parameter fluctuations against the noise for $N = 400$ and $L = 10$ ($\rho = 4$). The black line is a Gaussian fit of χ; it provides the average $\eta_c(\rho, L) = 0.56$ and the variance $\sigma = 0.10$

Suitably rescaling the curves in fig. 2.2 one can also evaluate the critical exponent β, as we roughly do in fig. 2.5.

In a similar way, one can write a scaling law also for the number density ρ. Even in this case the analogy with ferromagnetic systems leads to the expression:

$$\phi(\eta, \rho; L) = \begin{cases} \left(\dfrac{\rho - \rho_c(\eta; L)}{\rho_c(\eta; L)} \right)^{\delta} & \text{for } \rho > \rho_c(\eta; L) \\ 0 & \text{for } \rho < \rho_c(\eta; L) \end{cases} \tag{2.17}$$

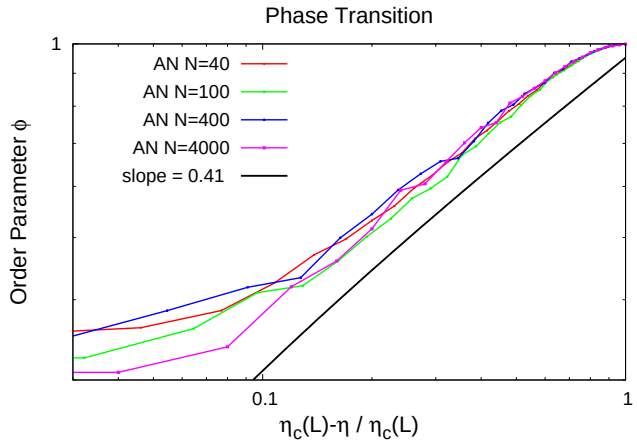

Figure 2.5: Evaluation of the critical exponent β. The curves represent different system sizes with same $\rho = 4$ (N=40, L=3.1; N=100, L=5; N=400, L=10; N=4000, L=31.6). The fit provides a value of $\beta \sim 0.4$, according with Vicsek estimation.

where δ is the critical exponent. In [10, 20] is reported an accurate evaluation of this critical exponent, either theoretically either through large scale simulations. On the contrary, we simply report in figure 2.6 the order parameter trend as a function of the density ρ for fixed value of the noise η. From the plot one can point out that, as expected from phenomenological considerations, the greater is the density of the system, the greater value is taken by the order parameter, or in other words, the greater noise is required to conserve the initial rotational symmetry.

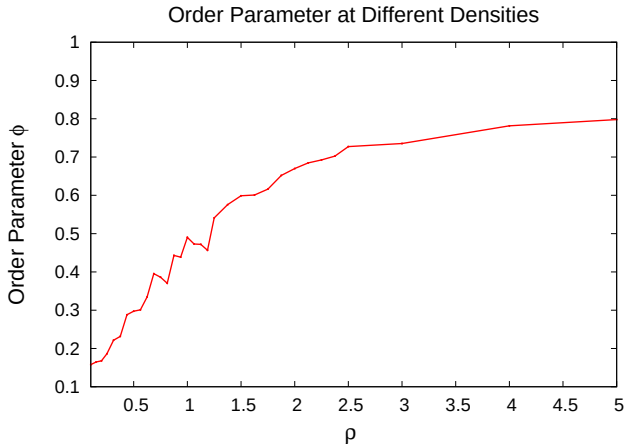

Figure 2.6: Plot of the order parameter ϕ as a function of the system density ρ for fixed value of the noise $\eta = 0.3$. Notice the analogy with ferromagnetic systems: the order parameter is higher for higher values of the system density.

Plotting $\phi(\rho; L)$ as a function of $(\rho - \rho_c(\eta; L))/\rho_c(\eta; L)$ is possible to estimate the value of δ. Since we are not going to perform large scale simulations, we refer to [10, 20] for further details.
As we have just observed, the value of η_c strongly depends on the system density ρ. In particular, higher values of the density ρ imply higher values of the critical value η_c. Theoretical and numerical considerations [20] suggest that the relation between the critical noise and the number density follows the power law:

$$\eta_c(\rho) \sim \rho^{\kappa} \tag{2.18}$$

with $\kappa = 1/2$ in $d = 2$. Our aim is not to find out the exact value of κ but, at least, check the validity of this relation in our results. We are going, indeed, to plot ϕ against η for different values of the density ρ and for fixed linear size $L = 20$ (fig.2.7).

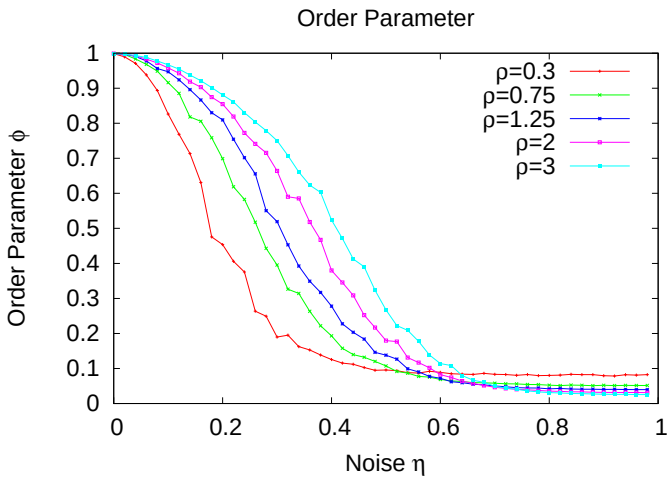

Figure 2.7: Plot of the order parameter ϕ versus the angular noise amplitude for different values of the density ρ and with $L = 20$.

If we rescale the curves in agreement with eq. (2.18), we obtain their collapse, as one can see in fig. 2.8.

The previous section wanted to show briefly that the statistical tools used by physicists are very powerful and useful even when applied to these kind of systems. Even though the Vicsek model is quite naive, it is very inclined to the physical point of view of the problem. Often, in physics, the simplest models are the most useful, or at least, a good base in order to describe a complex system. And also in this case, even if the starting point is really simple, it lends itself to a very powerful physical approach.

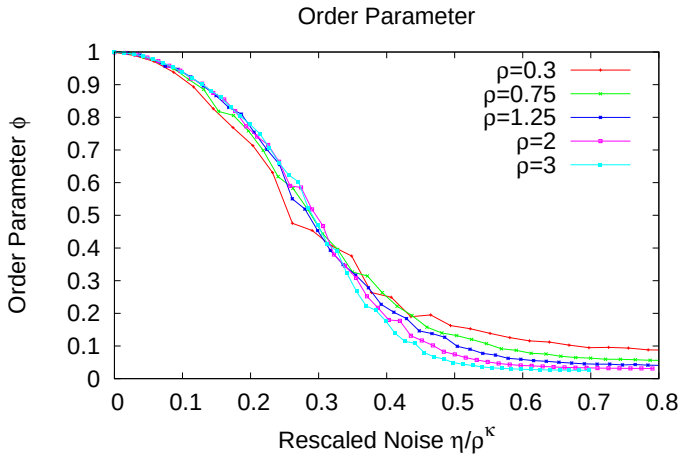

Figure 2.8: Plot of the order parameter ϕ versus the rescaled angular noise amplitude η/ρ^{κ} for different values of the density ρ and with $L = 20$

2.4 Clustering

One of the most characterizing features of this model is the formation of spectacular patterns such as fluxes and clusters. For enough low values of the noise, or at least lesser than the critical noise (for a given density), the "boids" join in two forms: flux, for null value of the noise, while clusters for $0 < \eta \leq \eta_c$. The former occurs when the interaction is purely deterministic, indeed after an initial transient the system breaks the rotational symmetry and a steady state showing a persistent flow is reached (fig. 2.9a). The latter occurs when the noise does not manage to preserve the symmetry but the motion is still stochastic (fig. 2.9b).

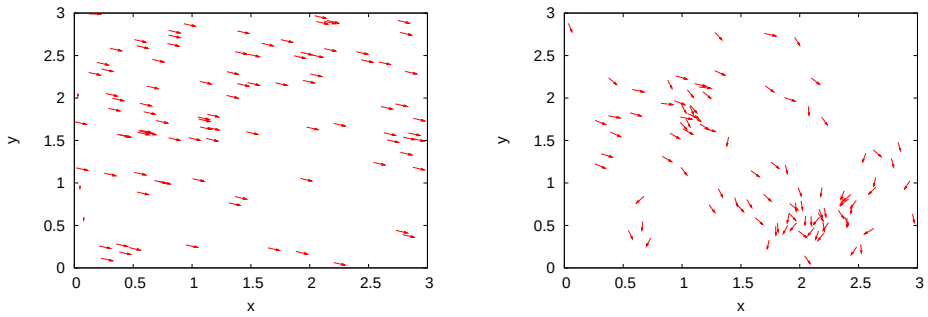

(a) **(b)**

Figure 2.9: Detail of a late system configuration snapshot for $\eta = 0$ and $\eta > 0$ respectively. The arrows point toward the last particle direction.

These two collective behaviours are very spectacular and worthy to be deeper studied. For this reason, inspired by [30], we are going to introduce and discuss the methods and the tools often used to describe the evolution of an isolated cluster.

We start by considering a situation in which all the particles are located at the origin and move towards $+\hat{\boldsymbol{x}}$ with speed v_0. For simplicity, we consider only angular noise perturbation acting on the system.
Since all particles see each other, we can simply describe this system within a mean field approach. Moreover, since all the particles start with the same direction, every time a particle calculates the average direction of its neighbours the results is again the direction $+\hat{\boldsymbol{x}}$. This involves two immediate consequences: the noise is a random perturbation around their common direction and we can see the average direction as an external field that guides all the particles.
In other words, the updating rule (2.1) can be seen as

$$\vartheta_i(t+1) = \alpha_0 + \eta\xi_i(t). \tag{2.19}$$

where, in this case, $\alpha_0 = 0$.
This means that the probability to find a particle pointing in direction ϑ is

$$P(\vartheta) = \frac{1}{2\pi\eta} g(\vartheta, \alpha_0, \eta) \tag{2.20}$$

with

$$g(\vartheta, \alpha_0, \eta) = \begin{cases} 1 & \text{if } \alpha_0 - \eta\pi \leq \vartheta \leq \alpha_0 + \eta\pi \\ 0 & \text{otherwise} \end{cases}$$

with $0 \leq \eta \leq 1$.
In order to simplify the problem we assumed that α_0 does not change over the time. it is an acceptable assumption in this situation since the leading orientation is α_0 itself. The position of the i-th particle at time $t_n = n\Delta t$ is then given by:

$$x_i(t_n) = \sum_{k=0}^{n} \cos\vartheta_i(t_k) v_0 \Delta t \tag{2.21}$$

$$y_i(t_n) = \sum_{k=0}^{n} \sin\vartheta_i(t_k) v_0 \Delta t \tag{2.22}$$

Using (2.21), (2.22) and (2.20) and remembering that $\xi_i(t)$ is a δ- correlated white noise uniformly distributed with zero mean ($\langle\vartheta_i(t_k)\vartheta_j(t_l)\rangle = \sigma\delta_{i,j}\delta_{k,l}$) it is possible to calculate the average positions $\langle x(t_n)\rangle$, $\langle y(t_n)\rangle$ and the variances

$$\mathrm{Var}(x(t_n)) = \langle x(t_n)^2\rangle - \langle x(t_n)\rangle^2 \tag{2.23}$$

and

$$\mathrm{Var}(y(t_n)) = \langle y(t_n)^2 \rangle - \langle y(t_n) \rangle^2. \tag{2.24}$$

where $\langle \dots \rangle$ represents the average over the N particles and the realizations of the noise. For instance

$$\begin{aligned} \langle x(t_n) \rangle &= \int_{-\pi}^{\pi} P(\vartheta) x(t_n) d\vartheta = \\ &= \frac{v_0 \Delta t}{2\pi\eta} \sum_{k=0}^{n} \int_{-\eta\pi}^{\eta\pi} \cos\left(\vartheta(t_k)\right) d\vartheta = \\ &= \frac{v_0 n \Delta t}{\pi\eta} \sin\left(\eta\pi\right) \end{aligned} \tag{2.25}$$

$$\begin{aligned} \langle y(t_n) \rangle &= \int_{-\pi}^{\pi} P(\vartheta) y(t_n) d\vartheta = \\ &= \frac{v_0}{2\pi\eta} \sum_{k=0}^{n} \int_{-\eta\pi}^{\eta\pi} \sin\left(\vartheta(t_k)\right) d\vartheta = \\ &= 0 \end{aligned} \tag{2.26}$$

$$\begin{aligned} \langle x^2(t_n) \rangle &= \int_{-\pi}^{\pi} P(\vartheta) x^2(t_n) d\vartheta = \\ &= \frac{(v_0 \Delta t)^2}{2\pi\eta} \sum_{l=0}^{n} \sum_{k=0}^{n} \int_{-\eta\pi}^{\eta\pi} \cos\left(\vartheta(t_l)\right) \cos\left(\vartheta(t_k)\right) d\vartheta = \\ &= \frac{(v_0 \Delta t)^2}{2\pi\eta} \sum_{k=l=0}^{n} \int_{-\eta\pi}^{\eta\pi} \delta_{k,l} \cos^2\left(\vartheta(t_k)\right) = \\ &= \frac{n(v_0 \Delta t)^2}{2\pi\eta} \left[\pi\eta + \frac{\sin\left(2\pi\eta\right)}{2} \right] \end{aligned} \tag{2.27}$$

$$\begin{aligned} \langle y^2(t_n) \rangle &= \int_{-\pi}^{\pi} P(\vartheta) y^2(t_n) d\vartheta = \\ &= \frac{(v_0 \Delta t)^2}{2\pi\eta} \sum_{l=0}^{n} \sum_{k=0}^{n} \int_{-\eta\pi}^{\eta\pi} \sin\left(\vartheta(t_l)\right) \sin\left(\vartheta(t_k)\right) d\vartheta = \\ &= \frac{(v_0 \Delta t)^2}{2\pi\eta} \sum_{k=l=0}^{n} \int_{-\eta\pi}^{\eta\pi} \delta_{k,l} \sin^2\left(\vartheta(t_k)\right) = \\ &= \frac{n(v_0 \Delta t)^2}{2\pi\eta} \left[\pi\eta - \frac{\sin\left(2\pi\eta\right)}{2} \right] \end{aligned} \tag{2.28}$$

Given these results at hand one can derive the diffusion coefficients of the spreading process of the cluster. Indeed we can write a sort of bi-dimensional Fokker-Plank equation for the density evolution of the cluster

$$\partial_t \rho(\boldsymbol{x}, t) = -V(\eta, v_0)\partial_x \rho(\boldsymbol{x}, t) + \nabla \cdot (\mathbf{D}(\eta, v_0)\nabla \rho(\boldsymbol{x}, t)) \tag{2.29}$$

with a convective term, calculated as the projection along the $\boldsymbol{x}$-axis of the instantaneous velocity

$$V(\eta, v_0) = v_0 \int_{-\pi}^{\pi} P(\vartheta)\cos\vartheta d\vartheta = v_0 \frac{\sin(\eta\pi)}{\eta\pi} = \lim_{t_n \to \infty} \frac{\langle x(t_n)\rangle}{t_n} \tag{2.30}$$

and a diffusive matrix $\mathbf{D}(\eta, t)$ having the form

$$\mathbf{D}(\eta, v_0) = \begin{pmatrix} D_x(\eta, v_0) & 0 \\ 0 & D_y(\eta, v_0) \end{pmatrix} \tag{2.31}$$

where

$$D_x(\eta, v_0) = \lim_{t_n \to \infty} \frac{\mathrm{Var}(x(t_n))}{t_n} = \left(\frac{1}{2} - \left[\frac{\sin \eta\pi}{\eta\pi} \right]^2 + \frac{\sin 2\eta\pi}{4\pi\eta} \right) v_0^2 \Delta t \tag{2.32}$$

$$D_y(\eta, v_0) = \lim_{t_n \to \infty} \frac{\mathrm{Var}(y(t_n))}{t_n} = \left(\frac{1}{2} - \frac{\sin 2\eta\pi}{4\pi\eta} \right) v_0^2 \Delta t. \tag{2.33}$$

It is worth to comment a couple of properties of $V(\eta, v_0)$ and $\mathbf{D}(\eta, v_0)$ emerging from this procedure

- Since
$$\lim_{\eta \to 0} V(\eta, v_0) \to v_0 \tag{2.34}$$
there is only a deterministic transport of particles (flux) toward $+\hat{\boldsymbol{x}}$ direction;

- Since
$$\lim_{\eta \to 1} V(\eta, v_0) \to 0 \tag{2.35}$$
the particles are completely uncorrelated and their behaviour is similar to a random-walk.

- For small values of noise
$$D_y > D_x \tag{2.36}$$
which means that the cluster has more spreading along the orthogonal to the direction of motion. This strongly suggest the formation of bands moving coherently.

It is worth to notice that his description is valid only for the time in which the cloud of particles remain one coherent cluster. This is no longer true for longer times. Indeed with the increasing of the cluster spread, it happens that not all the particles "see" all the others, and so the cluster can break in two or more parts.

The previous analytical procedure offers a good description of the cluster behaviour in a very, maybe too, simple situation. An interesting question could be what happens when more complex scenarios arise. Vicsek model sets, indeed, periodic boundary conditions and so the clusters cannot be considered isolated. Anyway, one could guess that the cluster spreading due to the stochastic noise and the random collisions between different clusters reaches a steady state in which the probability distribution to find a cluster with m particles becomes constant.
As a consequence we are going to define and investigate the "cluster size distribution"

$$P(m,t) = \frac{m n_m(t)}{N} \tag{2.37}$$

where $n_m(t)$ is the number of clusters with m particles at the time step t. Qualitatively, this observable is expected to be a monotonic decreasing function for high values of the noise, while is expected to be very peaked for high values of m when the noise is small. Fig. 2.10 shows the cluster size distribution in a system with $N = 200$ for different values of the noise.

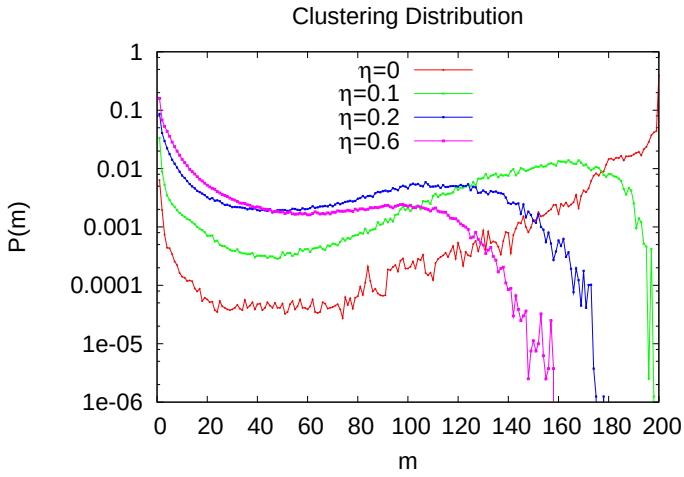

Figure 2.10: Cluster size distribution as a function of the size m (number of particles which form the cluster) for different values of the noise $\eta = 0.0$, $\eta = 0.1$, $\eta = 0.2$ and $\eta = 0.4$. To notice the peaks at large m for small values of η. We considered $N = 200$ and $\rho = 0.125$.

2.4.1 Clustering Algorithm

It is worth to notice that we consider a particle (j) belonging to the same cluster of (or connected to) another (i) if their distance is less than $2R$ and if its direction $\vartheta_j \in [\vartheta_i - 2\eta\pi, \vartheta_i + 2\eta\pi]$.
This choice is due to the fact that at each time step the particles are subjected to the random noise ξ that, in the worst scenario, adds or subtracts an angle equal to $\eta\pi$ to, or from, the average direction. As a consequence, if at the time t two particles are perfectly aligned and isolated, in the next time step they could be oriented toward two directions which differ for, at maximum, $2\eta\pi$. Since that they belong to the same cluster, the choice to use a gap of $2\eta\pi$ makes possible to recognize the cluster formed by these two particles. Otherwise, if the orientation of the j-th particle differ for more than $2\eta\pi$ it does not, obviously, belong to the same cluster.
A "cluster" is defined as an ensemble of connected particles, so it is worth to notice that it is not necessary that all the particles "see" all the others, but only that they interact at least with one of them. For instance, if one imagine three particles that do not interact with all of them, but the first and the third are inside a circle with radius $2R$ with center on the second, then the third particle is linked at the first through the second particle.

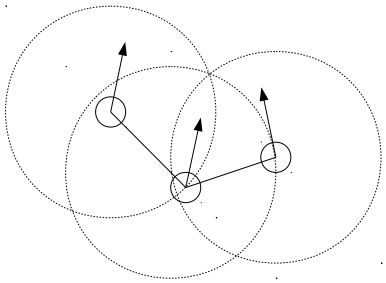

Figure 2.11: Example of linking algorithm used to recognize the clusters.

2.5 Giant Fluctuations

An other interesting aspect that characterize this model is the presence of "giant density fluctuations" [28, 29]. Let us consider a system undertaken Vicsek update rule and subjected to high values of the noise η. If we calculate

the density distribution in its subsystems, for instance squares, for increasing values of their linear size l we expect that the average number of particles inside the squares follows

$$\langle n \rangle \sim l^2_{square} \tag{2.38}$$

because high values of the noise make self-propelled particles move like Brownian particles, hence they reach an uniform density distribution within the system. In the same scenario, if one looks at the fluctuations of the number of particles, defined as

$$\mathrm{Var}(n) = \langle n^2 \rangle - \langle n \rangle^2 \tag{2.39}$$

whatever the density distribution is, $\mathrm{Var}(n)$ has to follow the following relation

$$\mathrm{Var}(n) \sim \langle n \rangle^{\alpha} \tag{2.40}$$

with $\alpha = \alpha_{gauss} = 1/2$ in the limit $N \to \infty$ and $L \to \infty$. This is because the Central Limit Theorem assures this relation for purely diffusing particles. On the contrary, if the system shows any type of correlation, α is no longer equal to α_{gauss}. In this section we are going to show that in suitable conditions, Vicsek model can reproduce giant density fluctuations, which mean high correlation among particles and cluster formation.
Since that in following chapters we are going to consider rectangular shaped systems, we are interested to study giant density fluctuations using anisotropic boxes, i.e. rectangular boxes. Indeed, for our purpose, it is more suitable to use rectangular boxes with fixed height $h = L_y$ and increasing base $l_{rect} \in [0, L_x]$ where L_x is the horizontal size of the system, as plotted in the picture below.

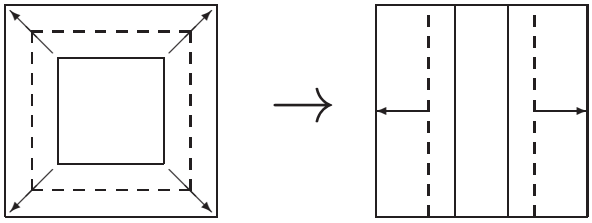

Since that the choice of rectangular boxes involves a different sectioning of the entire area of the system, we expect that the average number of particles inside each rectangular subsystem follows

$$\langle n \rangle \sim l_{rect} \tag{2.41}$$

instead of $\langle n \rangle \sim l^2$. Fig. 2.12 states the validity of this trend.

Even if the behaviour of $\langle n \rangle$ depends on the choice of how the boxes grow, because it is function of their linear size, $\mathrm{Var}(n)$ must be independent from this choice. Moreover, since the plots are made using the original Vicsek

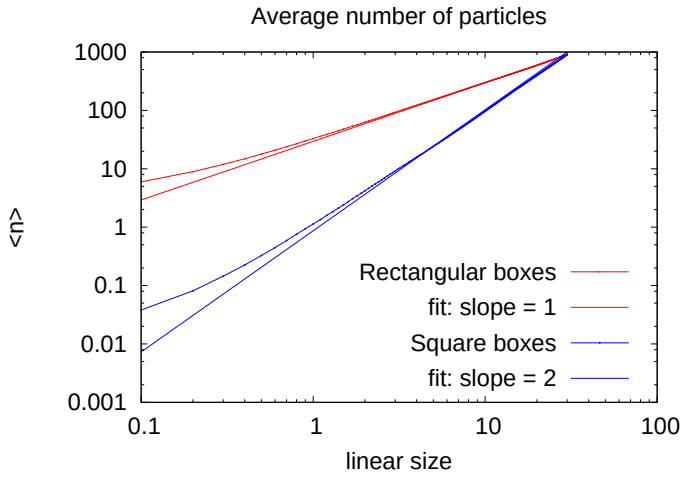

Figure 2.12: Average number of particles as function of the linear size of square or rectangular boxes. The system is a square with $L = 30$ and $N = 900$.

model with low values of the noise, we expect that the high correlation among the particles leads the systems to a state with non-uniform density, due to cluster and band formation. Or, in other words, we expect that the linear regression of $log(\mathrm{Var}(n))$ as a function of $log(\langle n \rangle)$ gives $\alpha > 1/2$. As shown in fig. 2.13 the giant density fluctuations exist and the linear regression gives $\alpha = 0.81$ that agrees with previous estimation of this exponent [29].

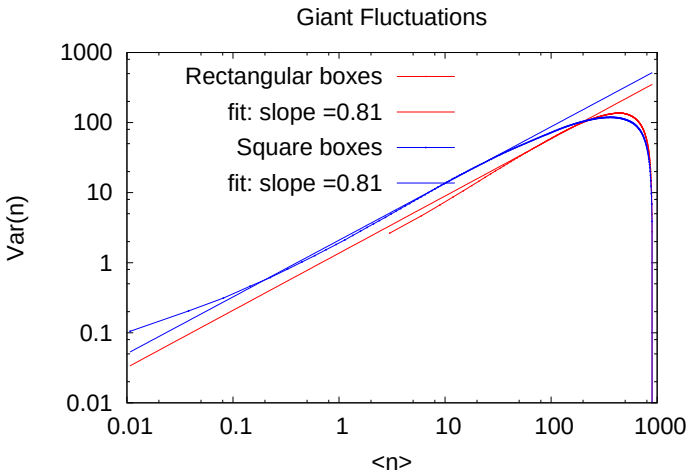

Figure 2.13: Giant fluctuations in a square system with $\eta < \eta_c$, $L = 30$ and $N = 900$ investigated with square and rectangular boxes.

For sake of completeness, in fig. 2.14 we report Var(n) as a function of $\langle n \rangle$ calculated using rectangular boxes in a system subjected to $\eta = 0.9$. In this case we expect and check the validity of the Central Limit Theorem in the Vicsek model subjected to high values of the noise.

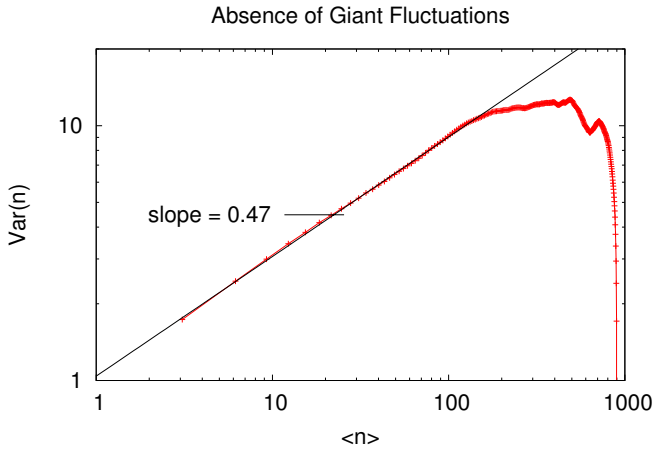

Figure 2.14: Absence of giant density fluctuations in a square system with $\eta = 0.9$, $L = 30$ and $N = 900$. The fit gives $\alpha = 0.47$ which agrees to α_{gauss} provided by the Central Limit Theorem.

2.6 The limit for low values of velocity

One of the most important parameter in the Vicsek model is the absolute velocity of the particles v_0. For null value of the absolute velocity the particles change their direction accordingly to the Vicsek update rule on ϑ, but, actually, they do not move. In other words, the system becomes a passive system, since that the activity defined by

$$\frac{d\,|\boldsymbol{v}|}{dt} = 0 \text{ with } |\boldsymbol{v}|\Big|_{t=0} = v_0 \tag{2.42}$$

is removed. One can identify this model with an off-lattice XY model for spin systems. In this case the system is no longer out-of-equilibrium and the Mermin-Wagner theorem states the impossibility for a two dimensional equilibrium system with continuous symmetry to show any type of symmetry breaking [31].
The test of this feature is very important to check the validity of the Vicsek model. In this respect fig. 2.15 states exactly that, for null value of the velocity, the phase transition is no longer showed.

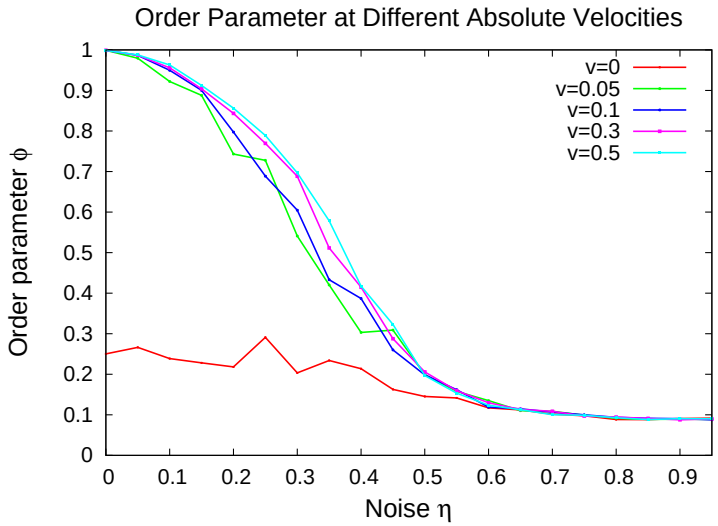

Figure 2.15: Plot of the order parameter in function of the noise for fixed value of density ($\rho = 1$) and for different values of the absolute velocity v_0.

The most important consideration to point out is that the role of the activity in this model is fundamental. Without activity the system looses all the amazing property which have in the original formulation. Even if the non-equilibrium state makes the model more difficult to work with, it is necessary in order to reproduce the features, like collective motions, which we are looking for.

One of the most important works which move toward this problem is Baglietto and Albano paper [22]. Here, the limit $v_0 \to 0$ is deeply studied in order to better understand the differences between the standard XY model and the Vicsek one. Understanding these differences means understand why the latter model shows a symmetry breaking, which is absolutely a non trivial problem. They discovered that the behaviour of the critical noise η_c as a function of the velocity v_0 takes a strange behaviour when the limit $v_0 \to 0$ is considered. Indeed, $\eta_c(v_0 \to 0)$ differs from the value taken when the velocity is chosen exactly equal to zero. In particular, they concluded that the combination of alignment interaction and displacement of the particles is essential for the existence of the phase transition. On the contrary, the mere fact that the system is off-lattice might not be responsible for the onset of the ordered phase.

3

Collective Motion of Hard-Core Spheres

Since that the aim of this thesis is studying collective motions in confining geometries, in this chapter we are going to modify the original Vicsek model and to consider round particles, i.e. particles which are hard 2D spheres, instead of point-like ones. Indeed, in order to fix properly the system size, we have to fix the volume of the particles. In fact, even if the system is not infinite, point-like particles can overlap each-other, and hence the system size would be meaningless.
Since that one of the most important parameters in the model is the interaction radius R, we choose to fix it as $R = 1$ (arbitrary unit) and to set the volume radius r with respect to this scale. Clearly, it must be $r < R$.
In order to do a choice with physical meaning we have to take into account that the existence of an excluded volume makes finite the number of possible interactions. Thus, we have to set a radius r that allows each particle to interact with not too few "flock-mates". For instance, if we set $0.25 < r < 0.5$ each particle would interact with only its first neighbours, because the second neighbours would not be seen by the particle. Even though this could be a reasonable choice, it would strongly reduce the interaction range. For this reason we choose $r \in (0, 0.25)$.

Collective motion in presence of finite-size objects was already investigated by Peruani et al. [32]. They pointed out the existence of a transition from the disordered state to the ordered one, in systems made of self-propelled rods. In this case the alignment rule is unnecessary, since that rod shaped objects have already a nematic interaction due to the geometry.
They proved, indeed, that in the case in which the aspect ratio of the rods is

equal to 1, i.e. the rods are squares, the particles do not perform collective motions and do not aggregate in ordered regions.
On the contrary, as far as we know, there are not any previous works regarding collective behaviours of finite size self-propelled particles interacting through an alignment rule like Vicsek one. For this reason it would be interesting studying how the observables defined in chapter 1 are affected by the introduction of the excluded volume.

The excluded volume is added to the system stopping, i.e. rejecting, the movement of a particle every time its volume would overlap the volume of an other, in other words, if the distance between the two center of mass is less than $2r$. In order to adopt this algorithm, we have to pay attention to the order in which the particles move. In other words, the update rule must be serial, indeed doing so, each movement of the i-th particle at the time step $t + \Delta t$ can be confronted with the position of the particle j at the time-step $t + \Delta t$ if $j < i$ and at the time-step t if $j > i$. On the contrary, it would not be so easy determine which particle has moved before an other[†].
More clearly, one can express this algorithm in formulae:

$$\boldsymbol{x}_i(t+\Delta t) = \boldsymbol{x}_i(t) \quad \text{if} \quad \begin{cases} [\boldsymbol{x}_i(t+\Delta t) - \boldsymbol{x}_j(t+\Delta t)]^2 < (2r)^2 & \text{for } j < i \\ [\boldsymbol{x}_i(t+\Delta t) - \boldsymbol{x}_j(t)]^2 < (2r)^2 & \text{for } j > i \end{cases}$$

3.1 Effects on Phase Transition

First of all, we are going to study the consequences brought by the introduction of the excluded volume on the phase transition behaviour. In this case we expect that the presence of the excluded volume involves more order in the system with respect to the same system but made of point-like particles. Indeed, if we consider a very dense system made of round particles, the geometrical contribution would be very relevant since that not all the possible directions are available. Actually, for fixed value of the noise amplitude, this system experiments a shrinking of the range of available directions. Moreover we expect that the greater is the density, the greater is this order effect. This feature can be seen in figures 3.1a - 3.2b.
As expected, the higher is the density ρ the more evident is the effect on the order parameter trend. Moreover, the higher is the volume radius, the greater values are taken by the critical noise $\eta_c(\rho, L)$ and the narrower are the order parameter fluctuations.

[†]This algorithm is strongly inspired by polymer units serial movements.

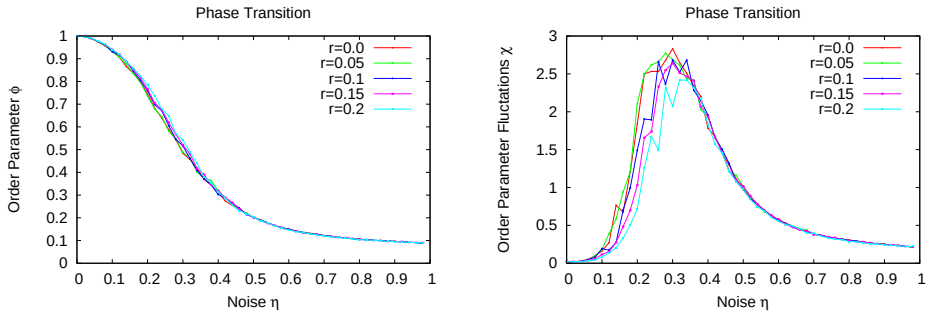

(a) Order parameter **(b)** Order parameter fluctuations

Figure 3.1: Plot of ϕ and χ as a function of the *angular* noise amplitude for different values of the radius r ($r = 0.0$, $r = 0.05$, $r = 0.1$, $r = 0.15$, $r = 0.2$) and at the same density $\rho = 1$.

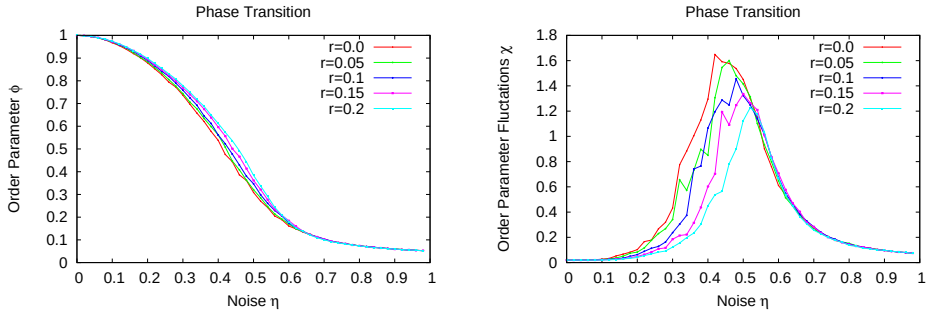

(a) Order parameter **(b)** Order parameter fluctuations

Figure 3.2: Plot of ϕ and χ as a function of the *angular* noise amplitude for different values of the radius r ($r = 0.0$, $r = 0.05$, $r = 0.1$, $r = 0.15$, $r = 0.2$) and at the same density $\rho = 3$.

In other words, the presence of the excluded volume strongly forces the particles to have a lesser fluctuating direction, and this effect is greater for higher density and higher values of the volume. As a consequence, the system results more ordered and more inclined to stay in this phase.
Since that in the previous plots systems subjected to angular noise were considered, now we are going to show how behave their counterpart, i.e. systems subjected to vectorial noise (fig. 3.3a - 3.4b).
This time the critical noise value is not shifted, but the order parameter fluctuations are still narrower for higher values of the radius r. This means that the introduction of the excluded volume in this types of systems involves more order for $\eta < \eta_c(\rho, L)$ but does not modify the inclination to stay in the ordered phase. The transition is definitely too sharp and disruptive to be affected by geometrical contributions.

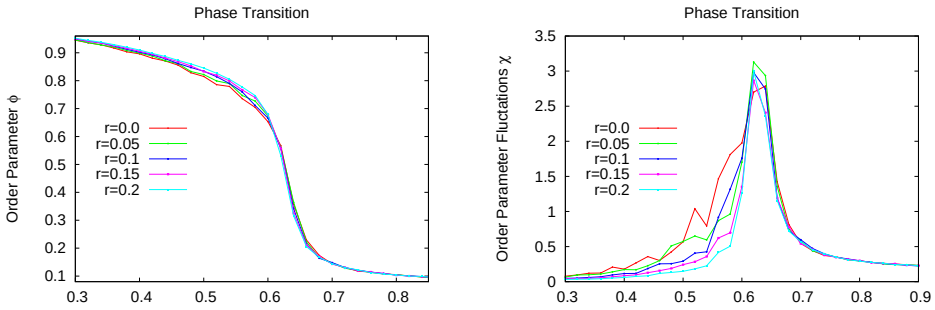

(a) Order parameter **(b)** Order parameter fluctuations

Figure 3.3: Plot of ϕ and χ as a function of the *vectorial* noise amplitude for different values of the radius r ($r = 0.0$, $r = 0.05$, $r = 0.1$, $r = 0.15$, $r = 0.2$) and at the same density $\rho = 2$.

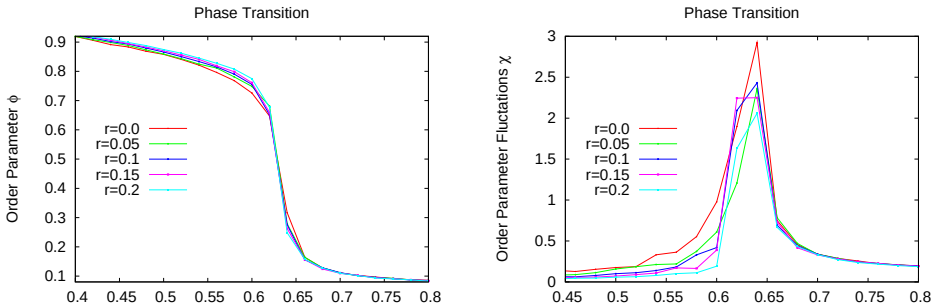

(a) Order parameter **(b)** Order parameter fluctuations

Figure 3.4: Plot of ϕ and χ as a function of the *vectorial* noise amplitude for different values of the radius r ($r = 0.0$, $r = 0.05$, $r = 0.1$, $r = 0.15$, $r = 0.2$) and at the same density $\rho = 3$.

3.2 Spatial Correlation

In this section we are going to introduce the 2D spatial correlation function $g(x, y)$ inspired by [14]. This observable is often used to estimate qualitatively the distribution of objects within the same cluster. For instance, in [14], $g(x, y)$ is investigated in order to check the nematic alignment among a population of bacteria. In that case the distribution stated that in systems made of rod-shaped objects, the probability to find two or more rod-shaped object along the orthogonal direction of the cluster is much greater than that along the longitudinal direction. In other words, the rod-shaped object

prefer to stay close side-by-side instead of head-to-tail.
In this work, we are not dealing with rods, but this observable could be useful to check some features of our model. First of all, it could check the validity of the algorithm used to consider the excluded volume of the particles. In next chapters we will see that we could use it also for other purposes. Let us then define the 2D spatial correlation:

$$g(x,y) = \frac{1}{\rho}\langle \sum_{j\neq i} \delta[x\hat{x}_i + y\hat{y}_i - (\boldsymbol{r}_i - \boldsymbol{r}_j)]\rangle_i \tag{3.1}$$

where $\langle ...\rangle_i$ represents the average over all the particles and the position difference $\Delta\boldsymbol{r} = x\hat{x}_i + y\hat{y}_i$ is expressed is i-th local frame. Fig. 3.5 shows two examples of $g(x,y)$ for systems made of point-like and round particles.

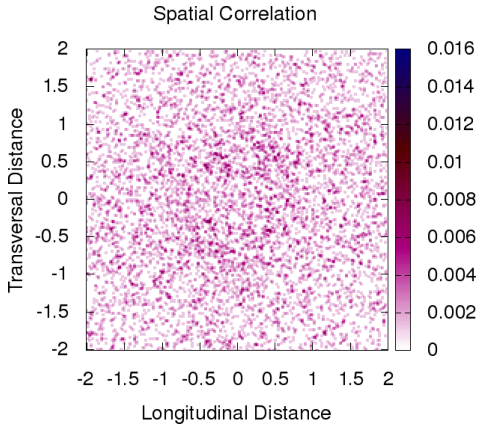

(a) $r = 0$

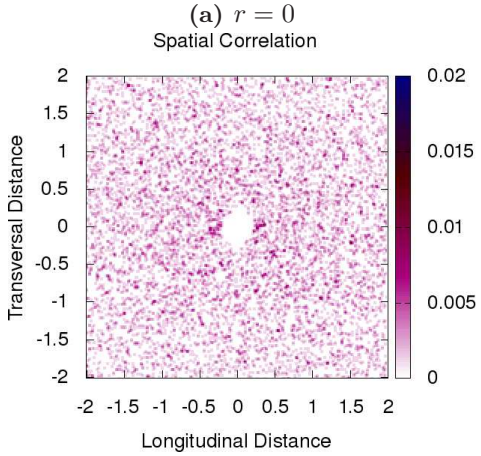

(b) $r = 0.1$

Figure 3.5: Plots of the spatial correlation $g(x,y)$ for systems with fixed $\rho = 1$ and $\eta = 0.1$ and for different values of the radius r. The hole in the right figure states the validity of our algorithm for the excluded volume.

4

Systems Confined in Stripes

Contents

In the previous chapters we have seen that the introduction of the excluded volume interaction brings some important consequences on the behaviour of the collective motion of self-propelled particles. In particular, we have pointed out that the presence of units with finite size pushes the system to be more ordered with respect to the corresponding one with point-like particles. In this chapter we want to focus on the consequences that confinement may have on collective behaviours. In particular, we are going to study collective behaviour of self-propelled particles with excluded volume confined in rectangular geometries. In the set up we considered the system as periodic along x-axis and sandwiched between two impenetrable walls located at $y = 0$ and $y = L_y$.

4.1 Bouncing Back Conditions at the Walls

In order to investigate the effects brought by the constriction we choose to let, for the moment, the system width $L_y = L_x$ and to shrink the width only at a later stage. The confinement is considered imposing a "bouncing back" conditions on the upper and lower walls. In other words, the two horizontal walls reflect the direction of those particles which try to cross them.
From the topological point of view, we are cutting the torus along $y = 0$ and reproducing a closed strip (or a 2d-channel) as narrower as smaller is L_y.

In order to fix the ideas we report a series of snapshots in which a system with $L_y = L_x = 10$ and $N = 100$ is subjected to different values of the noise. Fig. 4.1a and 4.1b show the onset of two separated fluxes flowing parallel and oppositely, respectively.

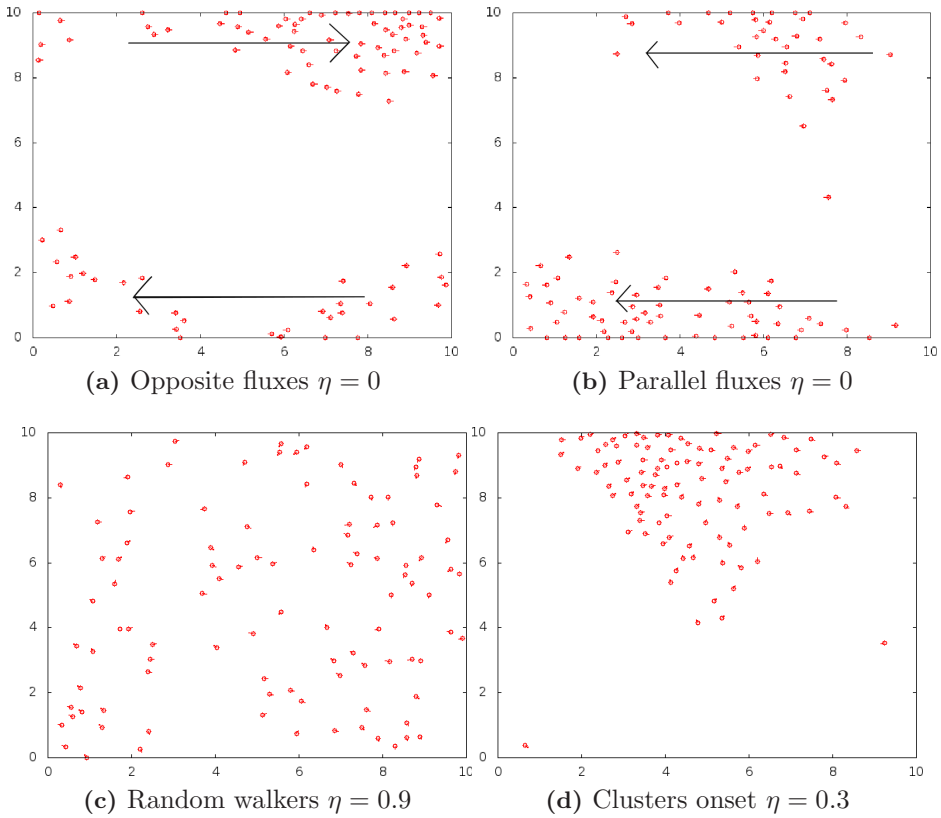

(a) Opposite fluxes $\eta = 0$ **(b)** Parallel fluxes $\eta = 0$

(c) Random walkers $\eta = 0.9$ **(d)** Clusters onset $\eta = 0.3$

Figure 4.1: Snapshot of different system behaviours for different values of the noise amplitude η. The system has $L_x = L_y = 10$ $\rho = 1$. The big arrows indicate the common direction of the flux.

This peculiar feature is due to the absence of noise. After few moments the particles reach a stable state flowing parallel to the walls. If the system is thick enough, as in this case, the upper and lower part could be completely detached from each other. Since that the order parameter we have defined is a global order parameter, this scenario causes a decrease of its value. This behaviour is obviously random but it is equally probable the production of one flux or two fluxes oriented to the same direction. Otherwise, we will see that for $L_y \sim R = 1$ such behaviour is not possible any more because the fluxes "see each-other" (the interaction range is comparable to the stripe width). So, the presence of isolated fluxes becomes lesser probable as narrower the stripe width decreases.
On the other hand, for increasing values of the noise, the particle do not manage to stay close to the walls because the noisy term. Indeed, for small, but non-null value of η, they prefer to join in clusters which, we will see further, are very inclined to stick to the walls (fig. 4.1d) but actually they do not persist for very long time close to the surfaces.
Fig. 4.1c shows an ensemble of particles subjected to $\eta = 0.9$. They perform random walks and are not affected by the presence of the walls.

A schematic idea of what happens to the particles in presence of bouncing back boundaries is shown in 4.2 and 4.3.

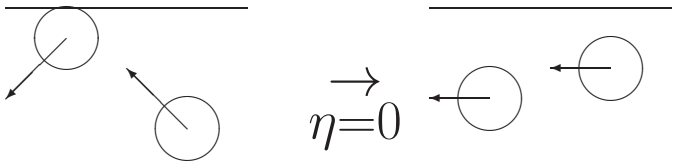

Figure 4.2: Scheme of the (deterministic) particles behaviour close to the wall for $\eta = 0$.

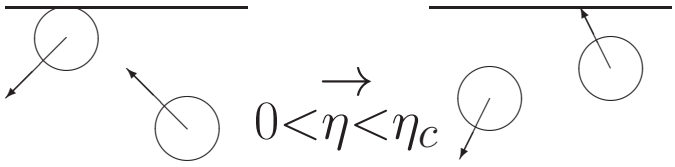

Figure 4.3: Scheme of possible particles behaviour close to the wall for $0 < \eta < \eta_c$.

Consider, for instance, two particles that do not interact each other but follow a quasi-common direction towards the wall. When the first particle hits the wall and inverts its direction the particles see each-other and interact. At this point there are two possibilities:

- if $\eta = 0$: they follow a common direction parallel to the wall;
- if $0 < \eta < \eta_c^{BB}(L)$ [†]: the particles interact but the noise is high enough to avoid the immediate alignment. So, most probably, also the second particle bounces over the wall.

In the following section we will study how these behaviours affects the system order parameter.

4.1.1 Effects on the Phase Transition

In this section we are going to compare the order parameter and order parameter fluctuations behaviours in presence of the confinement and in the original model. Fig. 4.4a and 4.4b show that the mere introduction of hard reflecting walls do not lead to a more ordered system, on the contrary it causes the enhancing of the high fluctuations range.

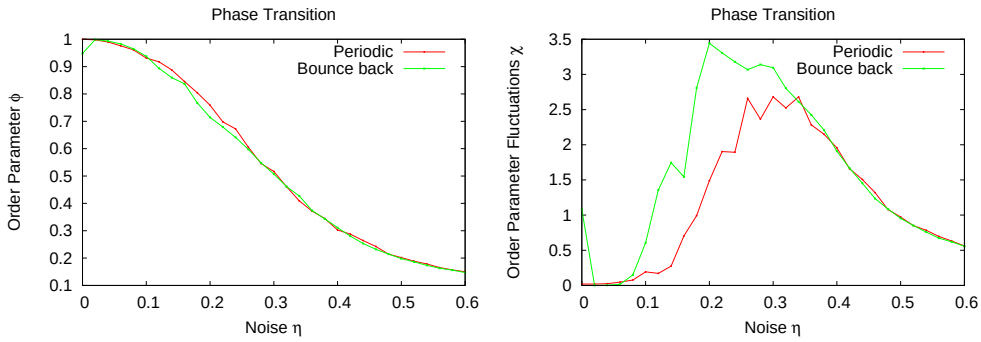

(a) **(b)**

Figure 4.4: Plot of ϕ and *chi* against η for periodic and bouncing back conditions in a system with $L_x = L_y = 10$ and $\rho = 1$.

Let us point out some comments about this scenario:

- For $\eta = 0$ one can notice that, as already mentioned in previous section, the order parameter is not equal to 1 because of the (random) formation of isolated fluxes with often opposite travelling direction.

[†] $\eta_c^{BB}(L)$ is the critical noise relative to the system with finite-size (L) and with bouncing back conditions on the walls.

- For $0 < \eta < \eta_c^{BB}(L)$ the presence of the confinement slightly decreases the order parameter value, on the contrary, the increasing of the fluctuations are very marked. This feature is due to the "bouncing" of big clusters. Indeed, while the first layers are reflected by a wall, the last ones keep pushing toward the wall. Doing so, many disordered configuration come up. Even though this process is only a transient between two ordered states, it takes as much time as bigger is the reflecting cluster.

- For large noise strength the curves are overlapped, indeed the walls do not play a relevant role on particles behaviour.

We will see that the size of the confined direction plays an important role on the system order. In particular, we expect that narrowing the size till $L_y \sim R$ will strongly affect the order parameter trend even for $\eta \gtrsim \eta_c^{BB}(L)$.

4.1.2 Density Distribution

In this part we want to point out the sticky effect due to the cluster-surface interaction. For null value of the noise the combinations of bouncing back conditions and deterministic dynamic caused the formation of fluxes parallel and noticed very close to the walls. In fig. 4.5 we compare the density distribution in the case of bouncing back and periodic conditions.

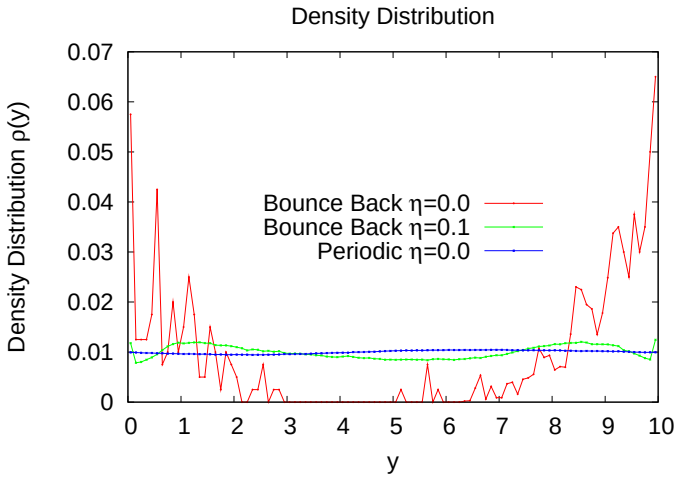

Figure 4.5: Plot of the density distribution profile $\rho(y)$ for systems with bouncing back, $\eta = 0$, bouncing back, $\eta = 0.1$ and periodic ($\eta = 0$) conditions. (The case with periodic conditions and $\eta = 0.1$ shows an uniform distribution as in the case for $\eta = 0$)

From this figure one can clearly infer that the particles have the tendency to stay close to the walls for null value of the noise when the constrained system is considered. On the other hand for $\eta = 0.1$, $\rho(y)$ is more uniform but still higher close to the boundaries. The sticky effect is not as relevant as is be in real bacterial systems, but we will see further that a more realistic effect can be reproduced slightly changing the boundary conditions.

4.1.3 Cluster Size Distribution

As already mentioned, we expect that the probability to find cluster with a large number of units increases when constrained systems are considered. The confining of environments leads naturally to larger number of interactions and to the onset of locally denser clusters. In this section we want to investigate the cluster size distribution $P(m)$ introduced in section 2.4 and compare the results with the unconstrained case.
Fig. 4.6 shows the cluster size distribution for $\eta = 0.1$ and $\eta = 0.2$ and for the constrained and unconstrained cases. As expected, the case in which the bouncing back boundary conditions are considered presents greater probabilities to find big clusters.

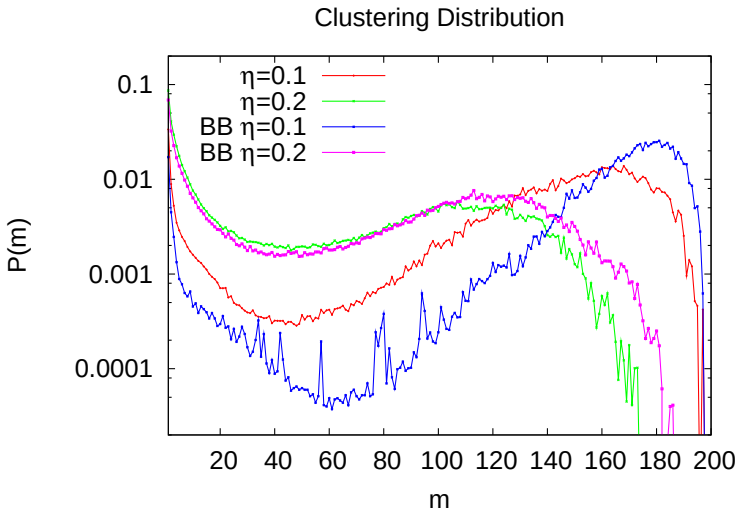

Figure 4.6: Plot of the cluster size distribution in the constrained and unconstrained cases for different values of the noise. Periodic: $\eta = 0.1$, $\eta = 0.2$. Bouncing Back: $\eta = 0.1$, $\eta = 0.2$.

4.2 Narrowing the Channel

In previous section we have introduced the confinement, but we let the system width ten times greater than the interaction radius R. In this section we are going to narrow the constrained dimension and to study the effects of *strong* confinement. We are indeed going to reduce the width L_y till values $L_y \sim R$ in order to confine the stripes in geometries very narrow and long. Below (fig. 4.7) we report some snapshots of the systems we are considering. Notice that the scales vary.

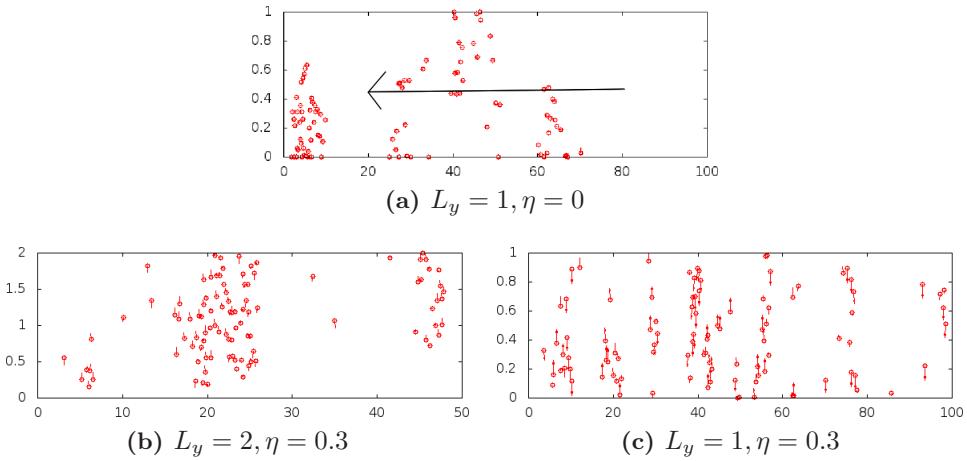

(a) $L_y = 1, \eta = 0$

(b) $L_y = 2, \eta = 0.3$

(c) $L_y = 1, \eta = 0.3$

Figure 4.7: Snapshot of system configuration for different values of system width and noise. The big arrow represent the common direction of the particles. Notice in fig. 4.7b and 4.7c the presence of big and small clusters respectively.

The first facts to notice are that, due to the strong confinement, the onset of oppositely directed fluxes is impossible. Moreover, small width increases the frequency of the interactions particle-surface. The onset of ordered states is made easier by the cluster width, which is forced to be as thin as L_y, this indeed involves a greater cluster mobility and inclination to stay aligned.
In the following section we are going to investigate quantitatively how the confinement affects the order parameter behaviour.

4.2.1 Effects on the Phase Transition

We have seen in sec. 4.1.1 that the introduction of hard walls has enhanced the order parameter fluctuations and decreased the order parameter value within the range $0 < \eta < \eta_c^{BB}(L)$. This is not what one expects from a constrained system. But, we will see in this section that the intuitive effect of the confinement (more order, tendency to stay aligned, etc.) shows up when one consider the geometry width of the same order of the interaction

radius R, i.e. strong confinement.
In the following figures (fig. 4.8 and 4.9) we compare the order parameter and the order parameter fluctuations of strongly and weakly constrained and unconstrained systems.

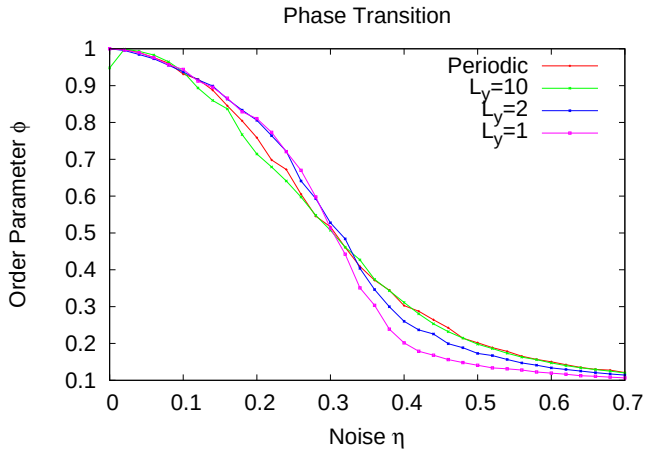

Figure 4.8: Plot of ϕ as a function of the noise η in constrained or unconstrained systems for fixed $\rho = 1$. Periodic: $L_y = 10$. Bouncing back: $L_y = 10$, $L_y = 2$ and $L_y = 1$.

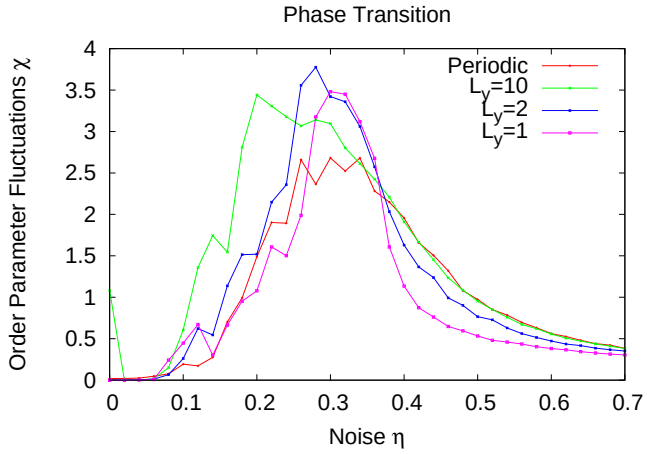

Figure 4.9: Plot of χ as a function of the noise η in constrained or unconstrained systems for fixed $\rho = 1$. Periodic: $L_y = 10$. Bouncing back: $L_y = 10$, $L_y = 2$ and $L_y = 1$.

The first features one can immediately point out from the figures 4.8 and 4.9 about the behaviour of ϕ and χ in systems with $L_y \sim R$ are:

- For $\eta = 0$ the order parameter must be equal to one. This is due to the impossibility of the formation of two isolated and oppositely directed fluxes (still possible for $L_y = 10$ as already pointed out).

- For fixed system size $A = L_x L_y$[†] and density ρ:

  - The critical noise $\eta_c(A)$ is shifted towards *higher* values of the noise.
  - The narrower is the channel, the narrower are the peaks of χ and the sharper is the order-disorder crossover.
  - χ experiences strong consequences of the presence of the constrain even for $\eta \gtrsim \eta_c(A)$.

As already mentioned, for strong confinement the cluster thickness is forced to be of the same order of L_y and hence, for small values of the width, the information spreading is very rapid and the cluster is very mobile. The immediate consequence is the increasing of the cluster coherence and of the order parameter ϕ. On the contrary, weakly constrained systems show big and lesser dense clusters through which the information does not move so fast. An other important effect is shown $\eta \sim \eta_c(A)$, indeed the order parameter experiences a very sharp decreasing. This feature is due to the great hitting frequency against the walls. Indeed, as soon as the noise is big enough, the clusters are subjected to fragmentation as we will see in sec. 4.2.3.

4.2.2 Density Distribution

Since that the strong confinement induced by bouncing back conditions at the boundaries pushes the particles to jump very frequently between the walls, we expect the density distribution to be more uniform with respect to the weakly constrained case. So, in this scenario, the sticky effect disappears more and more for smaller values of the confined direction size. This is clearly visible in fig. 4.10 where is plotted $\rho(y)$ for weakly (4.10a) and strongly (4.10b and 4.10c) confined systems.

[†]Since the linear size L_y and L_x vary, in this case the finite system size is considered fixing the area A. So η_c is determined for fixed A and ρ.

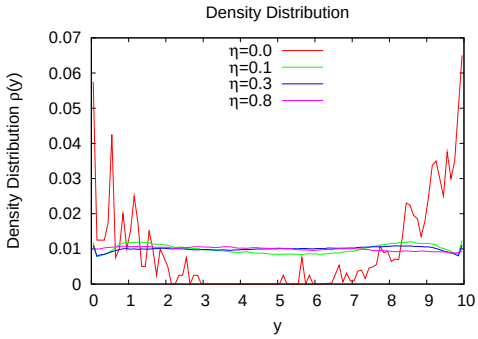

(a) $L_y = 10$

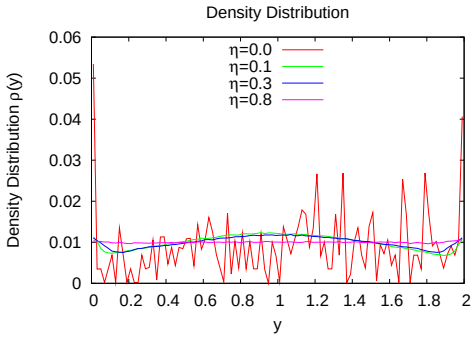

(b) $L_y = 2$

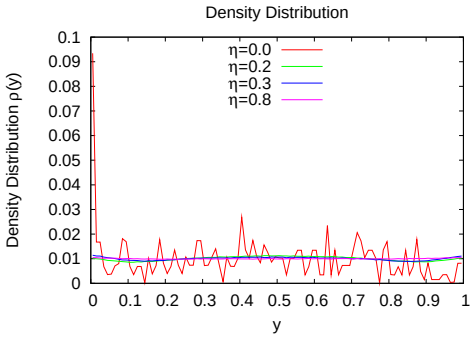

(c) $L_y = 1$

Figure 4.10: Plot of the density distribution projection on the y-axis for systems with different L_y and noises: $\eta = 0$, $\eta = 0.1$, $\eta = 0.3$ and $\eta = 0.8$.

4.2.3 Cluster Size Distribution

In previous section 4.2.1 we mentioned the onset of cluster fragmentation effect for $\eta \gtrsim \eta_c(A)$. Figure 4.11 is particularly indicative in order to make a point of such feature. For $\eta < \eta_c(A)$ the curves for the two values of L_y are quite similar so in the two cases the different values of the order parameter is not caused by the cluster dimension. On the contrary, as soon as the noise passes the critical value, the system with $L_y = 1$ shows greater probability to find smaller clusters with respect to the system with $L_y = 2$ and this contributes to the sharp decreasing of the value of ϕ in system with very small width. In other words the narrowing leads to the clusters fragmentation thus for fixed noise $\eta > \eta_c(A)$ the narrower is the strip, the more probable is to find smaller clusters which explain the shape of the curve of ϕ in fig. 4.9.

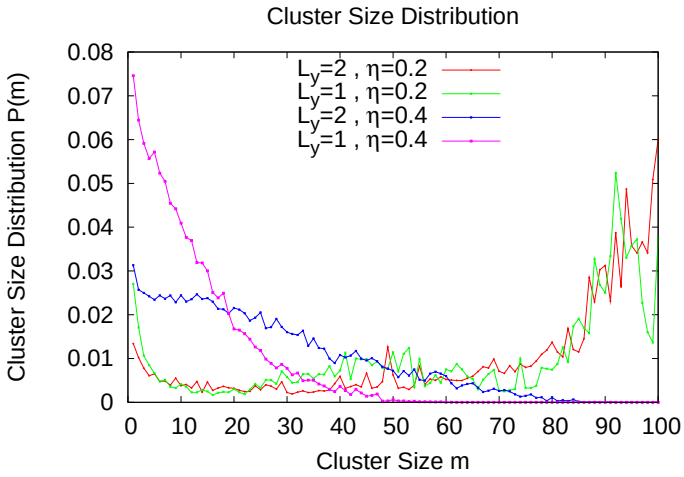

Figure 4.11: Plot of the cluster size distribution for a system with bouncing back conditions on the upper and lower boundaries and for different η and L_y values: $L_y = 2$, $\eta = 0.2$, $L_y = 1$, $\eta = 0.2$, $L_y = 2$, $\eta = 0.4$ and $L_y = 1$, $\eta = 0.4$.

4.3 Giant Fluctuations in Rectangular-Shape Systems

In this section we are going to show one of the most important achievements regarding confinement of active systems.
Indeed, we are going to point out that the giant density fluctuations already mentioned for the original Vicsek model, are also shown in constrained systems and they strongly depend on the size L_y. In figures 4.12a-4.12c are plotted $\mathrm{Var}(n)$ as a function of $\langle n \rangle$ for systems with different width and for $\eta = 0.1$ and $\eta = 0.9$. The data are provided through the same method described in sec. 2.5.
The worthiest fact to notice is that, for $\eta = 0.1$, the fit gives greater values of α[†] for lesser value of the system width L_y. In other words, the stronger is the confinement, the "more giant" are the density fluctuations. This feature suggest evidently the onset of strongly non-uniform states as moving bands. Notice that for $\eta = 0.9$ the systems show the expected behaviour for $L_y > 1$ ($\alpha \simeq 1/2$) but for $L_y = 1$ it seems that even with high noises the uniform density is not preserved. These results are, unfortunately, only preliminary and qualitative. Large scale simulations are imperative in order to state firmly the dependence of the giant fluctuations on the confinement strength. However, these plots strongly motivates further studies.

[†]Remember that α is defined as $\mathrm{Var}(n) \sim \langle n \rangle^{\alpha}$

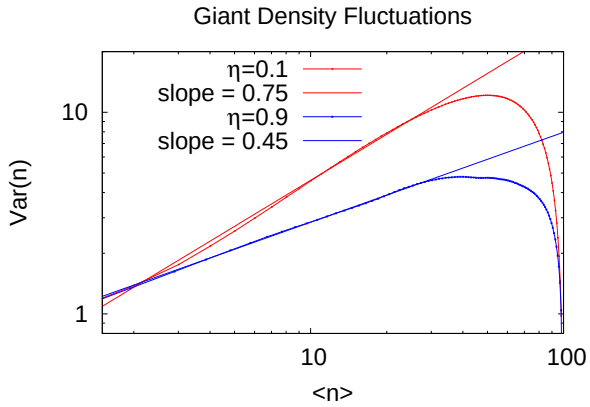

(a) $L_y = 10$

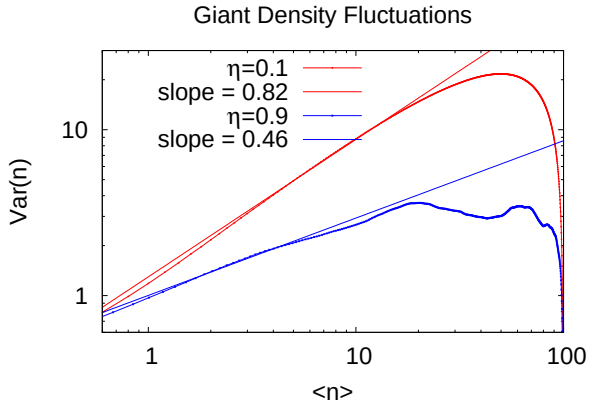

(b) $L_y = 2$

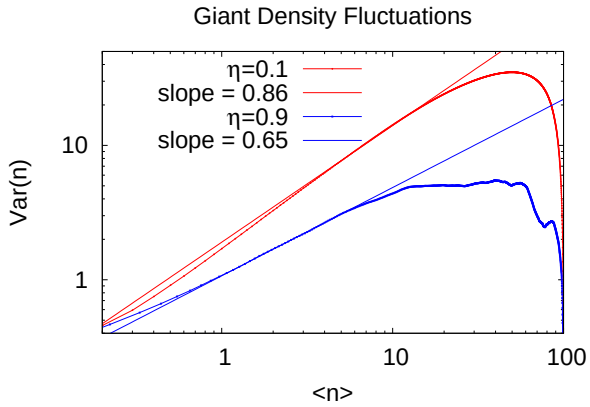

(c) $L_y = 1$

Figure 4.12: Plots of $\mathrm{Var}(n)$ as a function of $\langle n \rangle$ for a rectangular system with different widths and $\rho = 1$. The noise considered are $\eta = 0.1$ and $\eta = 0.9$.

5

Phenomenologically Inspired Boundary Conditions

Contents

In this chapter we are going to explore other boundary conditions at the walls $y = 0$ and $y = L_y$. These boundary conditions are phenomenologically inspired and tend to reproduce, in particular, the behaviour of living units that tend to avoid collisions with an obstacle. We consider:

Stop B. C.: In this case self-propelled particles stop their motion until they go a direction, caused by the noise or by the interaction with other particles, that would avoid a collision with the wall.

Slip B. C.: Here self-propelled particles slip along the boundary conserving their absolute velocity. This is closer to the behaviour observed in birds, bacteria and herds.

In particular, in this chapter we are going to study the effects that these conditions may have on density distribution, phase transition, cluster size distribution and density fluctuations in systems confined within stripes.

5.1 Stop Condition

In this section we are going to analyse new effects brought by the introduction of the "stop condition". In order to fix the ideas we plot below some snapshots of the typical system configurations at different times and with different noises.
In absence of noise, after few time steps, the system reaches a static (5.1b is equal to 5.1c) state in which all particles are blocked and aggregated in many little clusters (see fig. 5.1). Moreover we can just anticipate that the clusters have a pyramidal form: many particles lay on the wall while going far away from the boundary lesser particles are present.

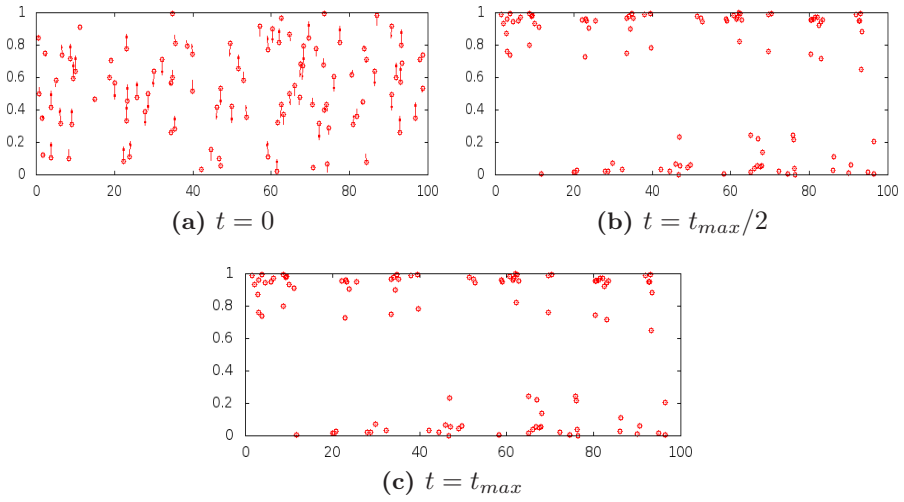

(a) $t = 0$ **(b)** $t = t_{max}/2$

(c) $t = t_{max}$

Figure 5.1: Snapshots of system configurations at different times and with noise $\eta = 0.0$. Notice the formation of stable pyramidal clusters. (Notice that the scales are unreal, in other words it seems that the particles are overlapping each-other and are moving only vertically but they are not.)

This configuration strongly suggest that the order parameter of the system can not be close to unity. Indeed the presence of many little (and isolated) clusters makes the particles only locally aligned.
On the other hand, if one increases slightly the noise, the situation is completely different. One can see in fig. 5.2 that there are metastable states in which large clusters occurs. In this condition we expect a greater value of the order parameter of the system with respect to the case with zero noise;

indeed there are more possibilities that the particles interact each-other during all time of the process.
In all these cases, however, we expect a non-uniform density distribution along the y-axis also in presence of noise (to be compared with results found in sec. 4.2.2). This means that our particles conserve the tendency to stay close to the walls until the noise strength reaches a sufficiently high value. This feature is quite similar to real bacteria behaviour which are trapped along the surfaces both because of the elongated shape of bacteria and of the hydrodynamic interactions [33, 34]. Even if real bacteria continue to swim along the walls, for now we are going to analyse this scenario as a middle-step to the introduction of the "slip" condition.

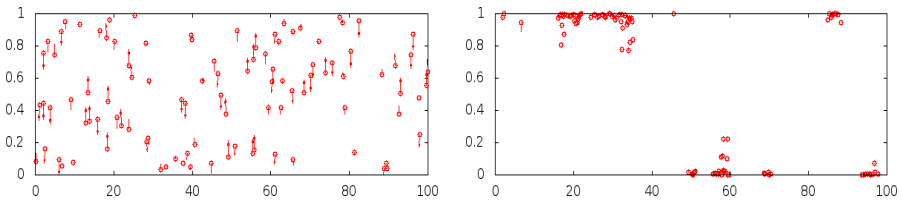

(a) $t = 0$ (b) $t = t_{max}/2$

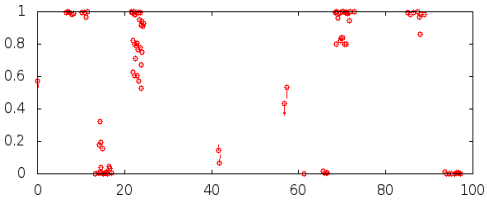

(c) $t = t_{max}$

Figure 5.2: Snapshots of system configurations at different times and with noise $\eta = 0.1$. Notice the metastable state in 5.2b characterized by the formation of big clusters. In fig. 5.2c the presence of pyramidal clusters are still observed.

5.1.1 Effects on the Phase Transition

As already mentioned the system configuration for null value of the noise is dominated by the presence of several non-interacting small clusters attached to the walls. Since the clusters are oriented upward or downward depending if they are on the upper or lower wall, these configurations correspond to low value of the global order parameter. This means that there is no longer a critical noise η_c for which for any $\eta < \eta_c$ the system reaches an ordered state. This is what one can point out from fig. 5.3 where one can compare the order parameter trend in stop and bouncing back boundary condition.

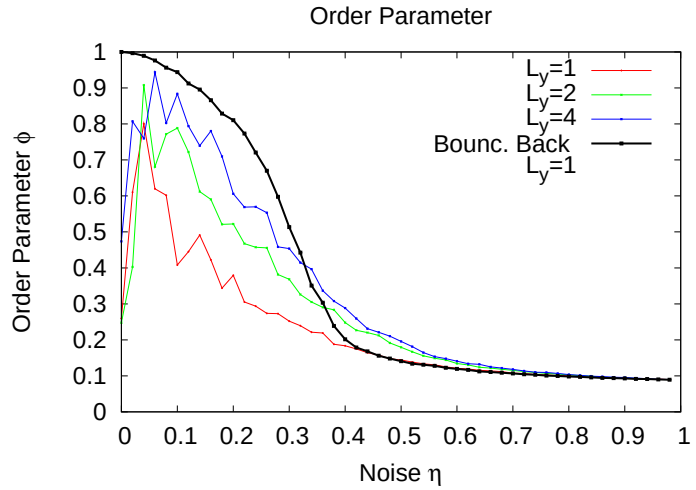

Figure 5.3: Plot of the order parameter as a function of the noise amplitude for different values of L_y and with fixed density $\rho = 1$ ($L_y = 1$, $L_y = 2$ and $L_y = 4$).

Another interesting point is the effect of the channel width on the order parameter trend.
In fig. 5.3 we report the order parameter as a function of the noise amplitude for different values of L_y. Since we have to maintain the same density, it is worth to notice that if we shrink the width, we also have to enlarge the strip's base (L_x). This means that there is a strong spread of particles along x-direction that could hinder the interaction among them especially if subjected to stop condition at the boundary because in this case free movements within the system are rarer.
From fig. 5.3 one can infer that for fixed value of the noise a smaller L_y implies a smaller value of the order parameter. A possible explanation is the following.
The boundary condition imposed is very strong, indeed every time one particle "hits" the wall it stops its motion; if now we focus on a single cluster, it is easy to understand that if the first layer is blocked near a wall, since the particles have a finite volume, all the other flock-mates are forced to stop in order to avoid overlapping.
For this reason the smaller the system width is, the more frequently the particles interact with the walls and consequently have to stop their motion. In other words the clusters have less "free path" between one stop and the other during which they can interact with other clusters. This means that the systems in channels present more but smaller clusters which move independently to the others, and so there is higher probability to find isolated clusters blocked in the two different walls simultaneously.
In the figures 5.4 and 5.5 are plotted two configurations of systems with

same density and different values of the width L_y.

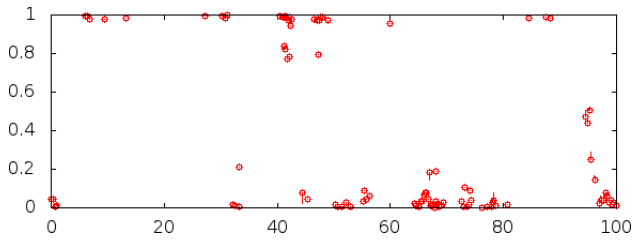

Figure 5.4: Snapshot of a configuration for system with $L_y = 1$ and fixed noise $\eta = 0.2$. To notice the presence of many and small independent clusters.

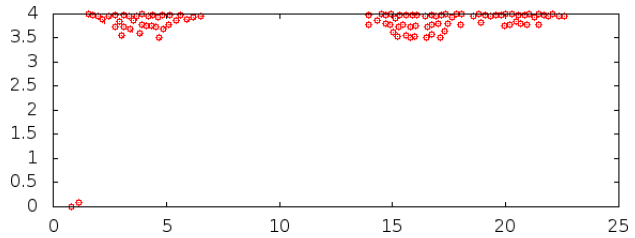

Figure 5.5: Snapshot of a configuration for system with $L_y = 4$ and fixed noise $\eta = 0.2$. To notice the presence of only two big independent clusters.

5.1.2 Effects on the Density Distribution

In this section we are going to discuss the increasing of the adhesion effect due to the introduction of the stop condition at the boundaries.
This feature is particularly interesting because reproduces phenomenological behaviours of self-propelled rod-like units. In [35] the authors underline the fact that only the elongated shape of the rods allows the aggregation at the side walls. Here we show that, with opportune boundary conditions, the aggregation (at the walls) is possible also with round particles.

In fig. 5.6 we show the density distribution along the y-axis for $\rho = 2$ and $L_y = 2$. In this scenario one can see the walls to act as "attractors"; indeed as soon as a particle interact with the surface it is literally frozen and its direction is, obviously, toward the wall. For this reason each particle that enters in its interaction radius R it is attracted to the "frozen" particle. Having in mind the process described above one has to investigate how the noise affects the configurations; if the noise is null the particles follow exactly the average direction of the "frozen" group and are stopped before

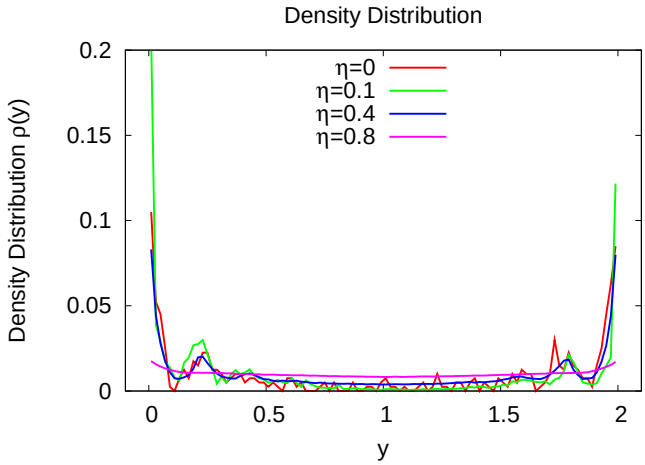

Figure 5.6: Plot of the density distribution as a function of the y-coordinate for fixed $\rho = 2$ and $L_y = 2$ and for different values of the noise ($\eta = 0$, $\eta = 0.1$, $\eta = 0.4$ and $\eta = 0.8$).

they would overlap their volume. So, as soon as a particle stops its motion it stays in that position for all time long of the process.
On the contrary, if the noise is big enough, the contributions of noise, alignment tendency and stop condition lead the group to rearrange itself until it reaches a stable configuration (a truncated cone, fig. 5.7).
For these reasons one can observe the red line in fig. 5.6 that is less sharp for $y = 0$ and $y = L_y$ and has several little peaks for half-values of the y-coordinate which represents the probability to find particles stopped by the tips of the triangular structures already formed. On the contrary for non-null but low values of the noise the density distribution reflects the tendency of the particles to fall as "avalanches" toward the near wall.

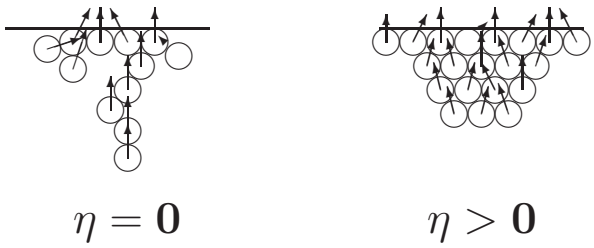

Figure 5.7: Examples of particle configuration for $\eta = 0$(left) and $\eta > 0$(right). The particle make advantage of the presence of the noise to rearrange their disposition in order to form the most stable configuration.

5.1.3 Cluster Size Distribution

In sec. 2.4 we defined the "cluster size distribution" $P(m)$ and we pointed out that in systems with periodic and bouncing back boundary conditions the probability to find large clusters is maximum for noises $\eta \in [0, \eta_c(L)]$. Moreover in sec. 4.2.3 we have highlighted that as soon as $\eta > \eta_c$ the combination of bouncing back conditions and narrowing of the stripes lead to clusters fragmentation. However, it is easy to understand that, for instance, bacteria do not bounce over the surfaces like balls. Otherwise, they could more inclined to stick on them and grow until a colony is formed.
In this work we do not allow the particle to reproduce but, by introducing the stop condition, we can fairly simulate the aggregation in colonies. For these reasons in this section we want to understand if the stop condition reproduces properly the feature of the bacteria to aggregate in precise locations.
We have already shown that for null value of the noise many and little long-living clusters are rapidly formed, while for little values of η the particles manage to form stable pyramidal structures. Obviously, the time needed by those structures to form is related to the channel width because for fixed noise the lesser is the width the more frequently the particles are stopped at the walls instead of interact each-other. In fig. 5.8 one can observe that the particles aggregate in a completely different way with respect to systems with previously boundary conditions.

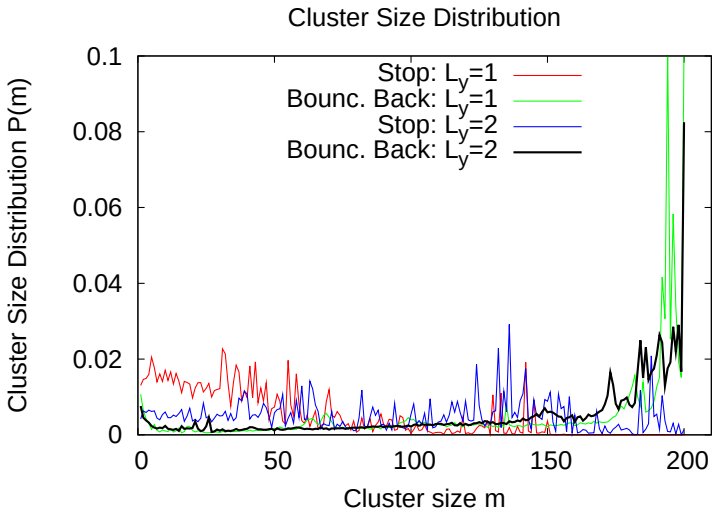

Figure 5.8: Comparison of the consequences between bouncing back and stop boundary conditions on the cluster size distribution for for fixed $\eta = 0.2$ and values of the width (Stop b.c.: $L_y = 1$, $L_y = 2$. Bouncing back b.c.:$L_y = 1$, $\mathbf{L_y = 2}$).

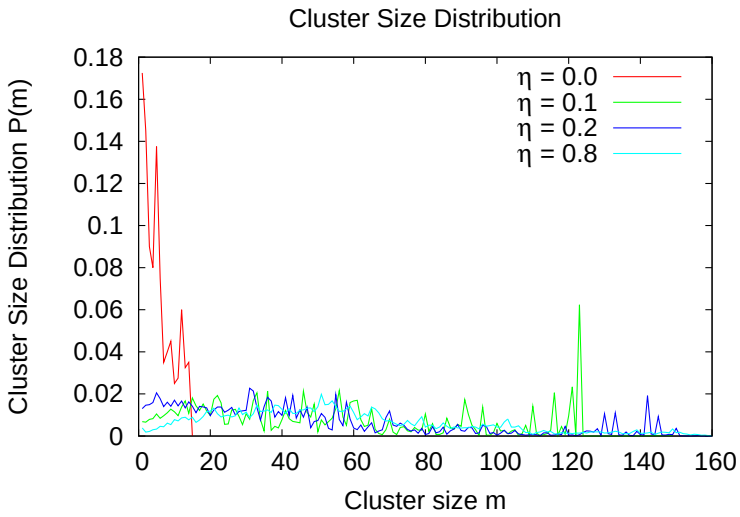

Figure 5.9: Plot of the cluster size distribution as a function of the cluster size m for fixed $L_y = 1$ and different values of the noise ($\eta = 0$, $\eta = 0.1$, $\eta = 0.2$, $\eta = 0.8$).

For instance, the two distributions for $\eta = 0$ with bouncing back and stop boundary conditions show that it is impossible to find big clusters in the latter case. Moreover, the greater aggregation effects arises for low, but non-null values of the noise (green line in fig. 5.9). This feature plenty satisfies what is experimentally observed: even if the bacteria live in noisy environment they are able to form stable structures stopping on the surfaces.
On the other hand the stop condition makes the units too less mobile, or in other words it is not very realistic that every time a bacteria hits a wall it stops its motion. Indeed it is more reasonable that the smaller vertical size should leads to more frequent interactions and should stimulate the onset of the self-organization instead of makes the particle less interacting.
A clue of this feature is shown in fig. 5.8, indeed for fixed noise the narrower is the system the greater is the probability to find smaller clusters. In sec. 5.2 we will introduce a different boundary condition in order to get over these difficulties.

5.2 Slip Condition

Strongly motivated by direct observation of bacteria interaction with obstacles [12] in this section we are going to reproduce the tendency of intelligent living units to avoid the hits with obstacles and at the same time to conserve the movement. We remind the "slip" condition:

Slip condition: Whenever a particle position at time $t + \Delta t$ would be beyond the upper or lower wall, the particle slips along the boundary conserving its absolute velocity v_0.

This condition is very suitable with respect to what is the aim of this work. Indeed, as stated in the introduction, we consider the particles non-reproducing and the environment, in which those particles move, filled of "food" homogeneously, consequently there are not biological motivations for which the units prefer a certain location. In this scenario we can investigate the system properties and the aggregation effect at the surfaces caused only by geometric contributions.

5.2.1 Effects on Phase Transition

Let us firstly investigate how this condition affects the order parameter trend. We expect that for low values of the noise the approaching to the stationary state is very rapid; indeed as soon as the i-th particle hits a wall its direction is immediately redirected along the border. After that, every particle entering in its interaction radius R is instantaneously and deterministically aligned to the i-th particle since that the latter is forced to move parallel to the wall. On other hand for higher values of the noise the slip conditions does not involve very different effects on ϕ with respect to the bouncing back conditions.

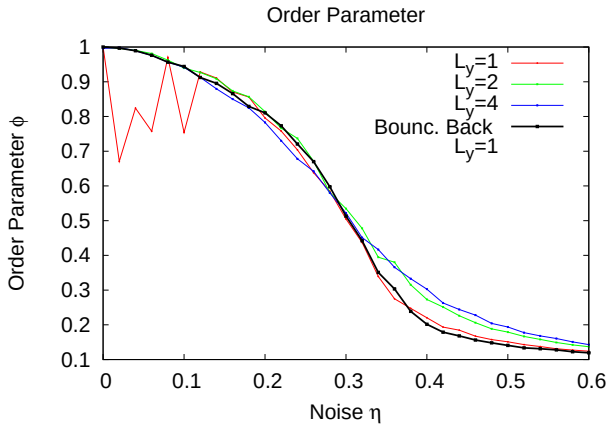

Figure 5.10: Plot of ϕ for fixed $\rho = 1$ and for different values of width L_y with slip condition ($L_y = 1$, $L_y = 2$, $L_y = 4$) and for **bouncing back , $\mathbf{L_y = 1}$** condition.

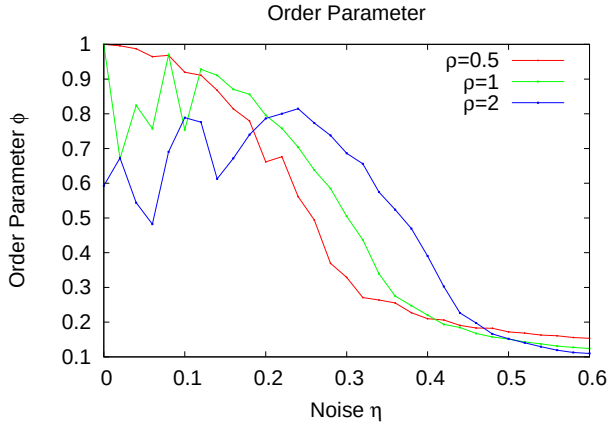

Figure 5.11: Plot of ϕ for fixed $L_y = 1$ and for different values of ρ ($\rho = 0.5$, $\rho = 1$, $\rho = 2$). Notice the enhancing of the unstable region at low values of η for increasing values of ρ.

From fig. 5.10 one can compare the trend of the order parameter in systems with different width L_y and for slip and bouncing back boundary conditions. It is evident that the curves for $L_y = 1$ in the case of slip (red) and bouncing back (**black**) boundary conditions are well-overlapped for η high enough. On the contrary, for low values of noise strength the slip conditions leads the system to unstable states in which the order parameter is not strictly close to one. From fig. 5.11 it is also clear that this strange behaviour is greater for bigger values of the system density. In order to understand the causes of this effect one can observe fig. 5.12. It shows that the dynamic of the system, which involves excluded volume and binding of the wall, leads the particles to "crystallize" in the structures shown in fig. 5.12a.

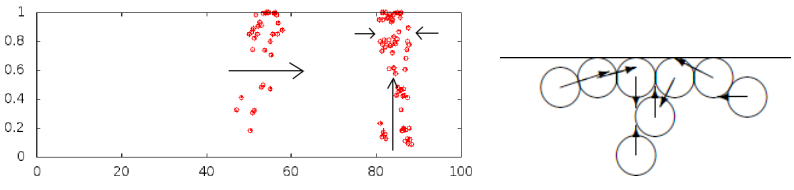

(a) **(b)**

Figure 5.12: (Left) Snapshot of a system configuration for $L_y = 1$. Notice that while the left cluster is moving rightward, the right cluster is blocked and static because of geometrical and dynamical reasons. (Right) Scheme of the dynamics that brings the particles to aggregate in static cluster.

5.2.2 Effects on Density Distribution

In this scenario the adhesion effect is still important but not so strong as in systems with stop conditions at the walls. Indeed the slip condition is less binding than the stop condition. The former reorients the particle direction parallel to the wall so that it is sufficient a little "push" of the noise toward the bulk to detach the particle from the wall. On the other hand, the particle frozen by the stop condition needs greater values of the noise strength to go far away from the boundary.
Since that the slip condition is less binding than the stop condition, we expect that for $\eta = 0$ the density distribution $\rho(y)$ takes high values close to the boundaries but as soon as η becomes non-null the slip condition loses rapidly its importance as one can infer from fig. 5.13.

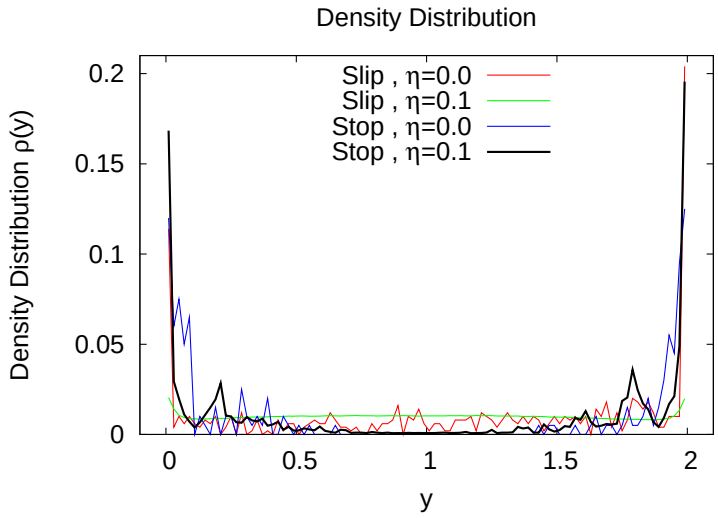

Figure 5.13: Plot of the density distribution projection along the y-axis for different values of the noise η and fixed width $L_y = 2$. Slip condition: $\eta = 0.0$ and $\eta = 0.1$. Stop condition: $\eta = 0.0$ and $\eta = \mathbf{0.1}$. While the red curve is still very peaked at the walls, the green curve represents the lack of persistent adhesion at the boundaries for $\eta > 0$.

5.2.3 Cluster Size Distribution

The cluster size distribution is a very good clue about what is the achievement reached through the introduction of the slip condition. Fig. 5.14a and 5.14b allow us to compare the effects on $P(m)$ of the stop condition and of the slip condition for different systems width and for $\eta = 0.2$ and $\eta = 0.4$ respectively.

What one can infer from these figures is that using the slip condition the "cluster fragmentation" pointed out for system with bouncing back conditions and also existent for stop condition is still present for values of η greater than the critical noise. This feature causes the rapid drop of the order parameter value for $\eta > \eta_c(A)$ observable in fig. 5.10 and as a consequence, the trend of ϕ is as sharper as smaller is the system width.
At the same time the slip condition involves high probability to find clusters with size $m \sim N$ for $\eta < \eta_c(A)$ while the stop one does not allow the cluster to aggregate in big clusters, as one can infer from fig. 5.14a.

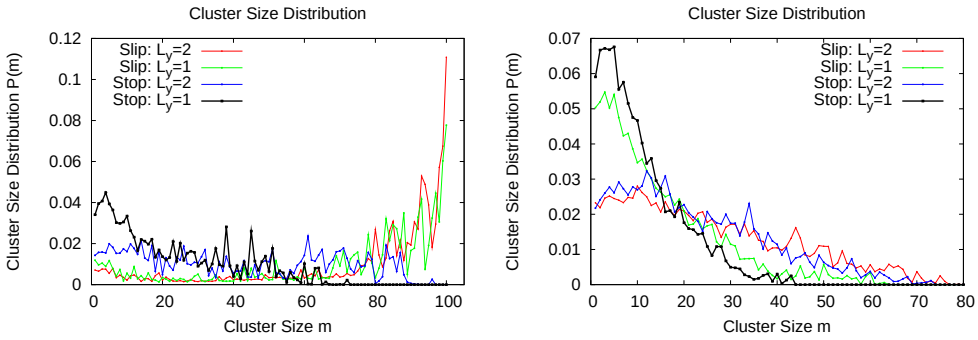

(a) $\eta = 0.2$ **(b)** $\eta = 0.4$

Figure 5.14: Plot of the "cluster size distribution" $P(m)$ as a function of the cluster size m for fixed noise η and $\rho = 1$. Different curves correspond to different values of the width L_y and boundary conditions. Slip condition: $L_y = 2$ and $L_y = 1$. Stop condition: $L_y = 2$ and $\mathbf{L_y = 1}$.

As a consequence, the slip condition is the most suitable boundary condition for our purpose. Moreover, it agrees with previous direct observations of bacterial systems and indirect observations of aggregation features.

5.3 Giant Density Fluctuations

Let us analyse how this boundary condition affect the density fluctuations. In sec. 4.3 we found that in systems subjected to strong confinement and bouncing back boundary condition, strong inhomogeneous configurations occur very frequently. Those giant density fluctuations were, moreover, directly related to the confined size of the environment.
In this section we want to investigate the giant density fluctuation when slip boundary condition is considered. To notice that, as far as we know, no one has ever tried to calculate this observable in real bacterial systems. On the

contrary, it is a good clue of the non-equilibrium state of the system. We show the results of our simulation in fig. 5.15.

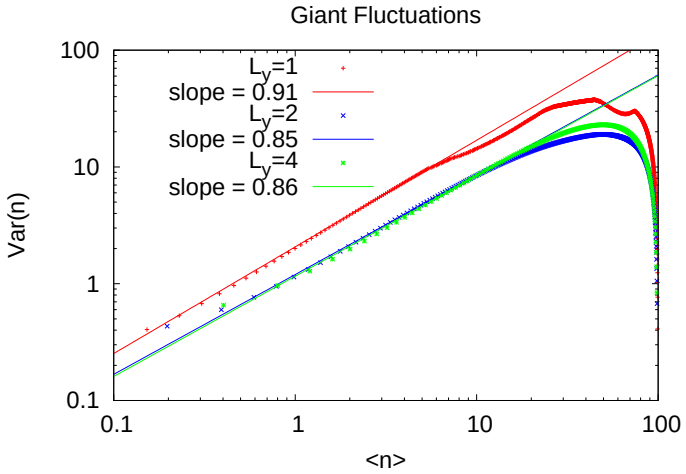

Figure 5.15: Plot of Var(n) as a function of $\langle n \rangle$ for systems with different width L_y and fixed noise $\eta = 0.1 < \eta_c(A)$ ($L_y = 1$, $L_y = 2$ and $L_y = 4$).

From the figure one can infer that the narrower the system is, the larger is the fluctuations. We remind that in the standard Vicsek model α was found to be $\alpha = 0.8$ [29]. Hence, even though we are not performing large scale simulations, the values we reported in fig. 5.15 and especially their dependence from the constrained size, strongly motivate deeper investigations regarding this topic.

6

Boundaries with Singularities

Contents

One of the main goal of this thesis is the study of the collective motion of self-propelled particles within confining non-differentiable geometries. We will restrict ourselves to simple non-differentiable geometries such as spikes and wedges.
The initial set up is made of N round particles with random positions and orientations within a system with periodic boundary conditions on the vertical borders and slip boundary conditions on the upper and lower walls which this time are not straight lines but present limited regions with positive (bottlenecks) or negative (wedges) curvatures (see fig. 6.1).

The aim of this chapter is to understand the interplay between the geometrical shape and the collective dynamic. Indeed, one of the main question we raised is: how is the collective motion affected by the confinement in irregular geometries? It is an important and interesting question and, as far as we know, not yet enough investigated. This topic gains even more

(a) Singularity with *negative* curvature **(b)** Singularity with *positive* curvature

Figure 6.1

prominence thank to technological developments which allow us to create microscopic strong constrained systems.
It is worth to remember that we are not considering the presence of food or other biological motivations. Hence, here we are interested only on the study of those geometrical contributions which could enhance the probability of trapping and clustering. For this reason, the final goal is to predict, for a given confining shape, the probability to find clusters of bacteria (or cells, metastasis ... whatever living or non-living unit describable by this model) in a certain region of the space-time.

6.1 Wedges

In this section we are going to simulate the presence of a wedge placed at the upper wall, while the lower one is kept straight (see fig. 6.1a). Note that the area of the wedge is very small with respect to the total system area A of the confined region. The wedge is parametrized by its half base w and slope α (the height is $h = w \cdot \alpha$). Giving an aspect ratio:

$$\mathcal{R} \equiv \frac{h}{2 \cdot w} = \frac{\alpha}{2}.$$

An interesting question to address for this geometry is whether, under suitable conditions of density and noise, the probability to find a large amount of bacteria inside the wedge is high even if they are not attracted by the presence of food. In order to do so we are going to study the density distribution inside the wedge as a function of the y-coordinate and the "residence time" T_{res} defined as:

$$T_{res} \equiv \frac{1}{T_{max}} \int_0^{T_{max}} \Theta(t) dt \tag{6.1}$$

where

$$\Theta(t) \equiv \begin{cases} 1 \text{ if } \int_{\mathcal{W}} \rho(x,y,t)dxdy \geq 0.1 \\ 0 \text{ , otherwise} \end{cases} \tag{6.2}$$

and T_{max} is the simulation time and the integral is performed inside the region $\mathcal{W}$ which represent the wedge. The resident time and $\rho(y)$ are going to be investigated for different values of the aspect ratio $\mathcal{R}$ and noise strength η. It is worth noticing that in this scenario the global order parameter ϕ loses its importance. Indeed also for low values of the noise it could happen that the particles inside the inlet are not aligned causing the decrease of the order parameter value. Moreover, in order to answer to the questions highlighted above we can use more powerful tools, as the density distribution, the residence time and the cluster distribution.

6.1.1 Density Distribution Inside the Wedge

In this section we look at the density distribution for different aspect ratio $\mathcal{R}$. The base of the wedge is fixed to $2 \cdot w = 3$. In other words the entrance of the inlet is fifteen times the diameter of the particles. It is worth noticing that larger $\mathcal{R}$ means higher curvature at the top of the wedge. As a consequence, we expect that for higher $\mathcal{R}$ the particles would be more inclined to "crystallize" at the top of the wedge.
Figures 6.3a-6.3d show the density distribution $\rho(h)$ as a function of the wedge's height h. These plots show, as expected, that the maximum of $\rho(h)$ is more shifted toward the top of the wedge for higher values of $\mathcal{R}$.
It is worth noticing that the domain of $\rho(y)$ in this case is $y \in [L_y, L_y + w \cdot \alpha]$. As a consequence, since we choose to let the normalization constant of $\rho(y)$ fixed to N, the curves plotted in figures *are not* normalized to 1. On the other hand, this choice can highlight another interesting information: the fraction of particles which explore, on average, the wedge at each time step. From these figures one can deduce that:

- when the noise is absent the particle are distributed quite homogeneously along the y axis but not along the x axis, or in other words they do not fill all the available space inside the wedge. This feature is due to the completely absence of the noise (fig. 6.2a). As soon as the noise is big enough, the particles begin to rearrange themselves in order to fill all the inlet's area. As a consequence many other particles can enter in the wedge and so all the cluster becomes trapped more efficiently (fig. 6.2b);

- for noises beyond the critical value $\eta_c(A)$ of the correspondent system *without* the wedge the distribution is more peaked towards the top of the wedge but a lesser fraction of particles explore, on average, the inlet at each time step. This is because the greater the noise is, the lesser the particles "feel" the inlet; as a consequence, it is harder for the particles to reach the top part of the wedge. However, 6.2c shows that once they have reached it, and the curvature is big enough ($\mathcal{R} > 1$), they are efficiently trapped, also for quite big noises;

- for noises $\eta \sim 1$ the particles are N random walkers and the particle take a diffusive behaviour. After enough time the particle reach a stable distribution in which the inlet is filled uniformly as the rest of the system (see fig. 6.2d).

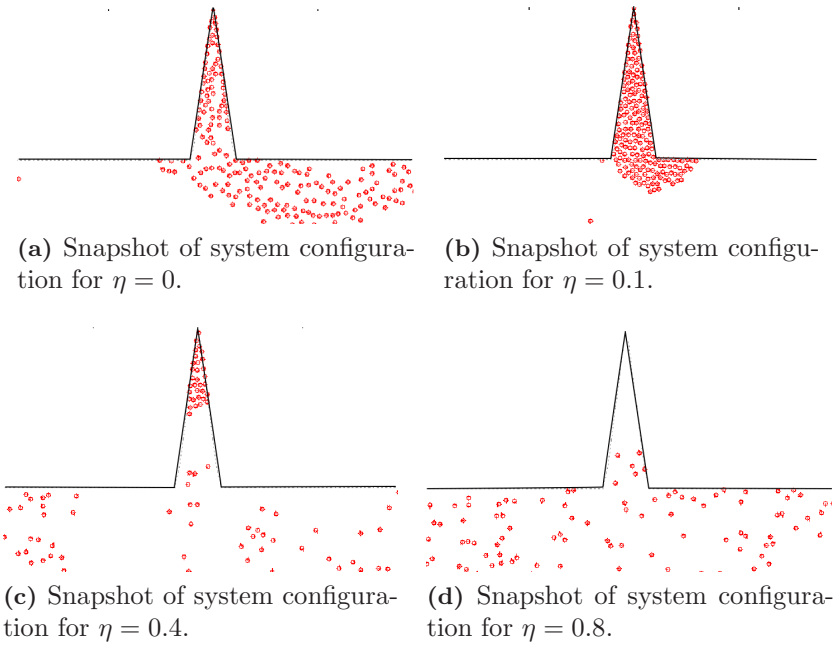

(a) Snapshot of system configuration for $\eta = 0$.

(b) Snapshot of system configuration for $\eta = 0.1$.

(c) Snapshot of system configuration for $\eta = 0.4$.

(d) Snapshot of system configuration for $\eta = 0.8$.

Figure 6.2: Notice the diverse way in which the wedge traps the particles depending on the noise strength. For $\eta = 0.1$ there is enough noise to permit the exploration of all the inlet. For $\eta = 0.4$ the combination of noise and wedge detach a group from the rest.

An interesting problem that arises from the considerations above concerns in estimating the "critical aspect ratio" $\mathcal{R}^*$ that is the value of $\mathcal{R}$ that, for a given noise strength, the trapping of the particles is efficient. Indeed, from figures 6.2a-6.2d one can point out that for fixed η, it exists a value $\mathcal{R}^*(\eta)$ for which a fraction of the particles are trapped inside the inlet and are completely uncorrelated from the rest of the system. In other words, it seems

that "as soon as those particles enter in the inlet, it closes behind them" as shown in fig. 6.2c.

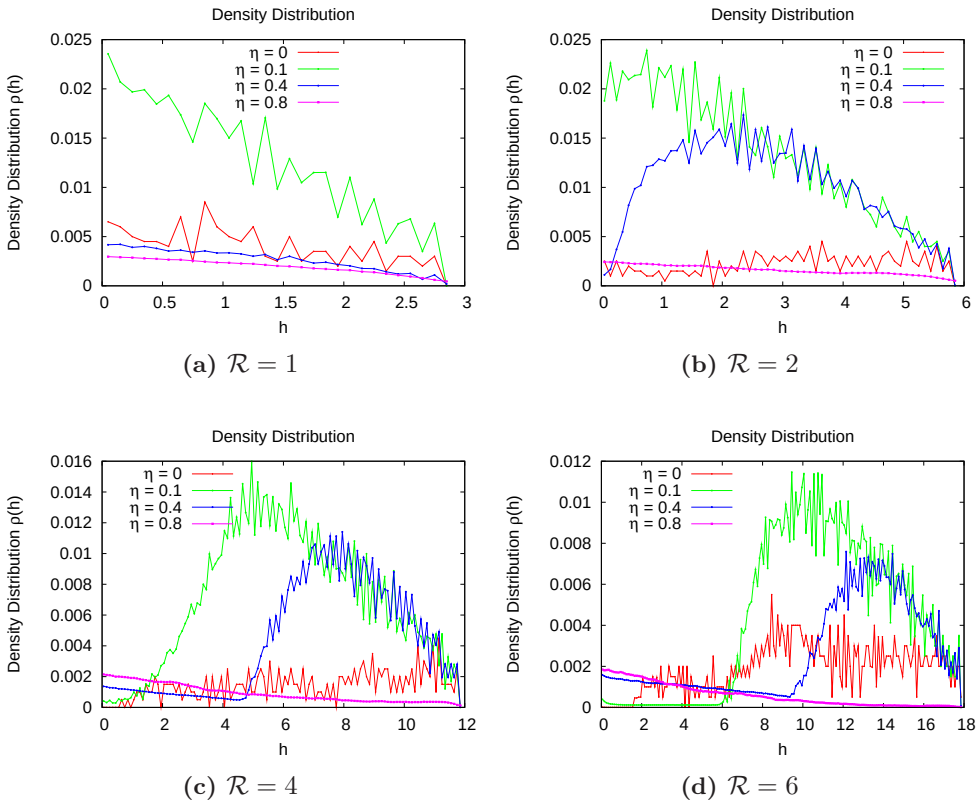

(a) $\mathcal{R} = 1$ (b) $\mathcal{R} = 2$

(c) $\mathcal{R} = 4$ (d) $\mathcal{R} = 6$

Figure 6.3: Plot of density distribution $\rho(h)$ as a function of the cone height h for fixed $\rho = 2$ and for different values of the noise η ($\eta = 0.0$, $\eta = 0.1$, $\eta = 0.4$ and $\eta = 0.8$).

6.1.2 Residence Time

In this section we are going to study the residence time defined in eq. (6.1). This observable has a very important meaning in this scenario since it indicates the time fraction during which more than the 10% of the particles are inside the inlet, for a given density ρ, noise η and aspect ratio $\mathcal{R}$. Fig. 6.4 shows the trend of T_{res} as a function of the noise η for different aspect ratios $\mathcal{R}$. The interpretation of the figure is quite straightforward but not trivial: for $\eta < 0.5$ the curves are well defined and not very noisy. In that range, one can observe that the sharper the wedge is the higher noise strength is needed to decrease T_{res}. This feature, in this particular range of noise,

makes a point of what already said in the previous section: sharper wedges assure a more efficient trapping.
For noises $\eta > 0.5$ the situation is slightly different, since particles are more similar to random walkers than flock-mates. In this case the residence time cannot give us any information about the trapping efficiency of the inlet with a certain aspect ratio.

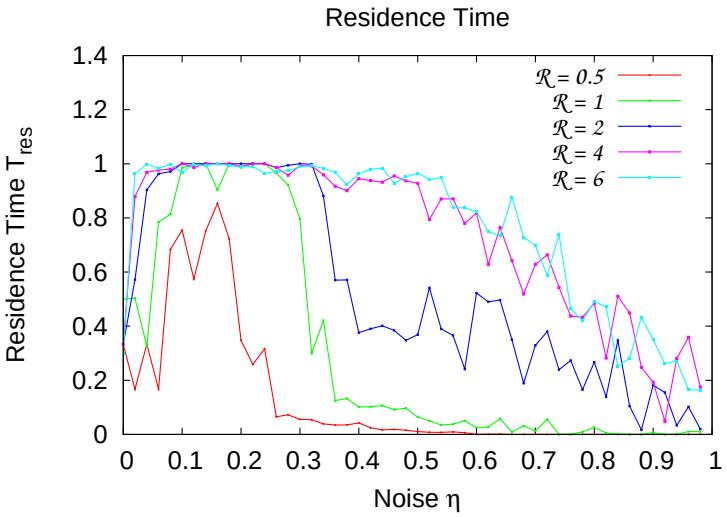

Figure 6.4: Residence time T_{res} as a function of the noise η for different values of the aspect ratio $\mathcal{R}$ and for fixed $\rho = 1$ ($\mathcal{R} = 0.5$, $\mathcal{R} = 1$, $\mathcal{R} = 2$, $\mathcal{R} = 4$ and $\mathcal{R} = 6$). Data are averaged over the last $5 \cdot 10^3$ configurations and over 10 different initial conditions.

Another important consideration is that, for aspect ratio $\mathcal{R} \leq 2$ and for $\eta < 0.5$, the residence time experiences a sudden drop for precise values of η, while higher aspect ratios do not lead to this effect.
This observations strongly suggests the existence of a "critical aspect ratio" $\mathcal{R}^*$ that, for this range of noise, can assure the presence of a certain amount of particles for a certain period of time.
Moreover, in an indirect way, the rapid decrease give us an estimation of the trapping efficiency of the wedges. Indeed, for fixed aspect ratio exists a critical noise $\eta^*(\mathcal{R})$ for which the wedge does no longer trap the particle in an efficient way.

Cluster Size Distribution

We expect that the cluster size distribution is strongly modified by the presence of the wedge. Indeed, as already pointed out, for not too big values

of the noise, the sharper the inlet is the more efficiently the particles are trapped and more time they spend inside it.
In particular we expect that for low values of $\mathcal{R}$ the cluster size distribution would be quite similar to that in the case of rectangular smooth systems (with the same width L_y). This is well confirmed in fig. 6.5.

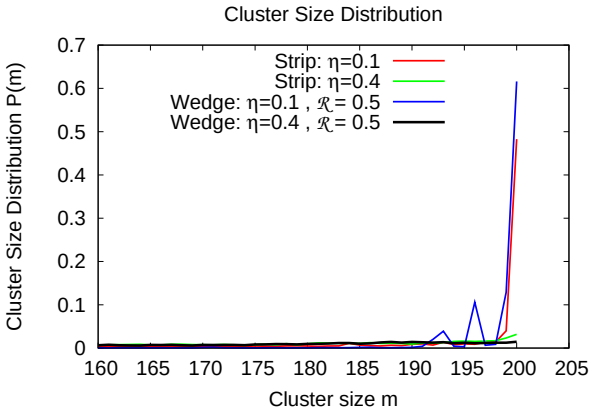

Figure 6.5: Plot of $P(m)$ for different values of the noise η, aspect ratio $\mathcal{R}$ and system geometry. Rectangular system: $\eta = 0.1$, $\eta = 0.4$. System with wedge: $\eta = 0.1, \mathcal{R} = 0.5$, $\eta = 0.4, \mathcal{R} = 0.5$.

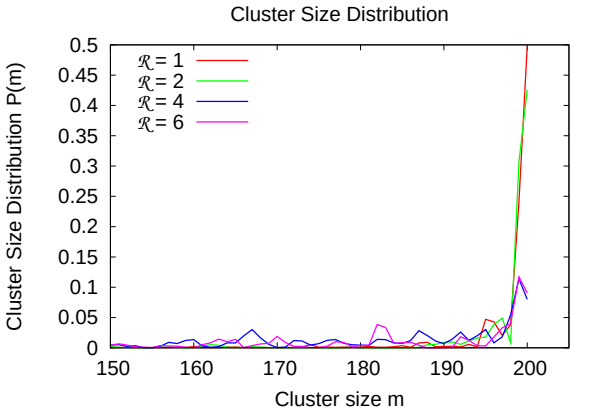

Figure 6.6: Plot of $P(m)$ for different values of the aspect ratio $\mathcal{R}$ ($\mathcal{R} = 1$, $\mathcal{R} = 2$, $\mathcal{R} = 4$, $\mathcal{R} = 6$). Notice the decreasing of $P(m \sim N)$ for greater values of $\mathcal{R}$ and at the same time the coming up of peaks for $m \lesssim N$.

On the other hand the introduction of sharper wedges brings stronger consequences on the clustering. For instance, as shown in fig. 6.6, the cluster size distribution at $m \sim N$ is less peaked for greater values of $\mathcal{R}$. At the

same time, it becomes more probable to find clusters having size m slightly smaller than N. This feature is another indication that sharper wedges imply greater probabilities to find a non-negligible fraction of particles inside them.

6.2 Bottlenecks

The aim of this section is to reproduce size irregularities frequently present in constrained biological and artificial systems. The investigation of this topic is, as already said, very suitable with respect to modern experiments regarding physics at the nanoscales.
Firstly, we are going to investigate the density distribution and the residence time as a function of the x-coordinate. Indeed, while in the previous section we were interested in the study of the trapping performed by the wedge (negative curvature), here we expect to observe other kinds of effect provided by the presence of obstacles with positive curvature. In particular, the presence of the wedge broke the spatial symmetry on the y direction, which suggested a careful investigation of the observable dependence on y coordinate. Now, the presence of the bottlenecks restores the x, y symmetry, so we are going to study both x and y dependences.

In order to fix the important quantities we remind that in this scenario the lower and the upper walls are functions of the x-coordinate. So we define

$$\mathcal{S} \equiv \min \{UpperWall(x) - LowerWall(x)\}. \tag{6.3}$$

We are going to consider $\mathcal{S} \in [0.5, L_y]$ which correspond to set the minimum gap large enough to allow the simultaneous passage of two particles in the former case and of $L_y/(2 \cdot r)$ particles in the latter (which corresponds to a system without constrictions).

6.2.1 Blockage Effect

In this scenario we expect that when the opening $\mathcal{S}$ is very small, it would obstruct the passage of the round particles. As a consequence, a sort of queue close to the most narrow space between the walls would arise. In order to check this effect, which is a very realistic phenomenon (one can think at the occlusions performed by cholesterol molecules in the veins), we study the density distribution ρ as a function of the x-coordinate. Next, we are going to study how long, on average, they stay in this configuration.

Density Distribution

As expected we observe a non-uniform density distribution along the x-axis. As the opening decreases $\rho(x)$ splits in two symmetric peaks, which is very reasonable, since we are considering a symmetric constrain (fig. 6.7, 6.8). The third plot (6.9) shows $\rho(x)$ for different values of the noise and for the same value $\mathcal{S} = 1$.

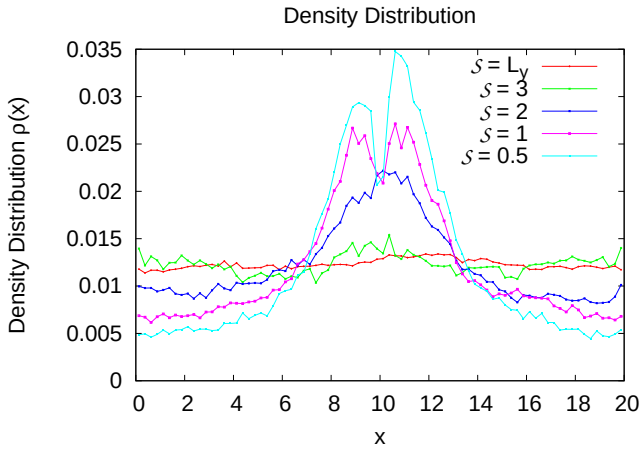

Figure 6.7: Plot of $\rho(x)$ for different values of the spacing $\mathcal{S}$ at fixed noise $\eta = 0$ ($\mathcal{S} = L_y$, $\mathcal{S} = 3$, $\mathcal{S} = 2$, $\mathcal{S} = 1$, $\mathcal{S} = 0.5$). (Notice that the bottleneck takes the minimum space between the walls at $x = L_x/2$)

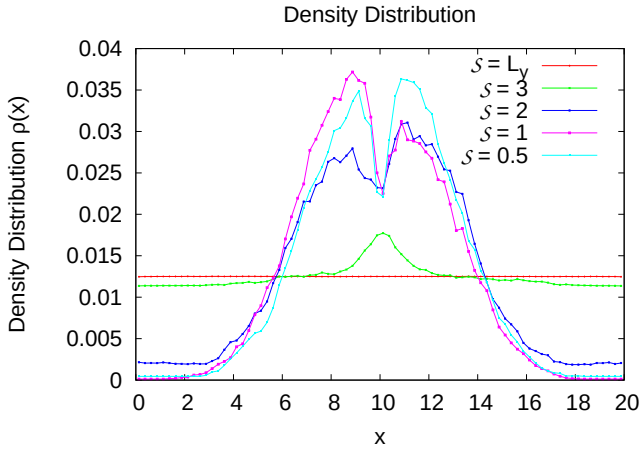

Figure 6.8: Plot of $\rho(x)$ for different values of the spacing $\mathcal{S}$ at fixed noise $\eta = 0.1$ ($\mathcal{S} = L_y$, $\mathcal{S} = 3$, $\mathcal{S} = 2$, $\mathcal{S} = 1$, $\mathcal{S} = 0.5$). (Notice that the bottleneck takes the minimum space between the walls at $x = L_x/2$)

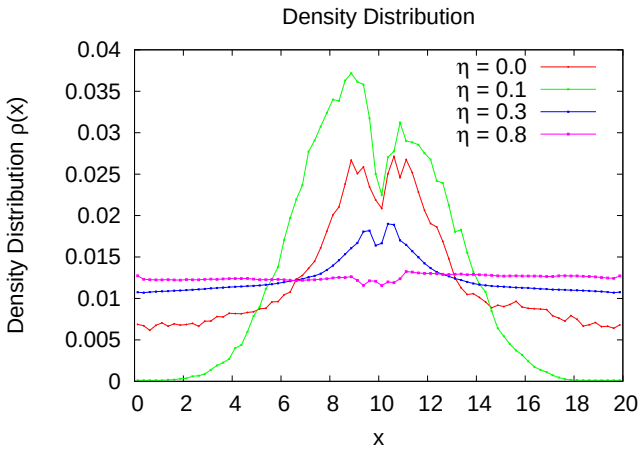

Figure 6.9: Plot of $\rho(x)$ for different values of the noise η and for fixed spacing $\mathcal{S} = 1$ ($\eta = 0$, $\eta = 0.1$, $\eta = 0.3$, $\eta = 0.8$). (Notice that the bottleneck takes the minimum space between the walls at $x = L_x/2$)

One can clearly observe the increasing of the inhomogeneity for smaller values of the spacing $\mathcal{S}$ and of the noise η. This means that the role of the blockage becomes very relevant for small values of the gap and for little values of the noise. On the other hand, we will see in the following sections that small gaps and little noises involves an interesting "focusing effect" on the particles. For these reasons it could be very stimulating to find the suitable conditions for which the blockage effect is minimum but this "focusing effect", which we will define better in next sections, is maximum. We will try to define the most appropriate observables and to answer to this question later in this chapter.

Residence Time

As already mentioned before, in this section we are going to investigate the resident time along the x-axis. The introduction of the constrain causes the particles to slow or stop their motion when they are close to the narrowest section. As a consequence a queue is rapidly formed. The aim of this section is to understand how long, on average, more then the 10 % of the particles are blocked close to the bottleneck. With this respect we define:

$$T_{res} \equiv \frac{1}{T_{max}} \int_0^{T_{max}} \Theta(t) dt \tag{6.4}$$

where

$$\Theta(t) \equiv \begin{cases} 1 \text{ if } \int_{\mathcal{B}} \rho(x,y,t)dxdy \geq 0.1 \\ 0 \text{ , otherwise .} \end{cases} \tag{6.5}$$

This time the region of the integration in eq.(6.5) is the range $\mathcal{B} = [0, L_y] \oplus [L_x/2.0 - w, L_x/2.0 + w]$. The residence time as a function of the noise for different values of the spacing $\mathcal{S}$ is plotted in fig. 6.10.

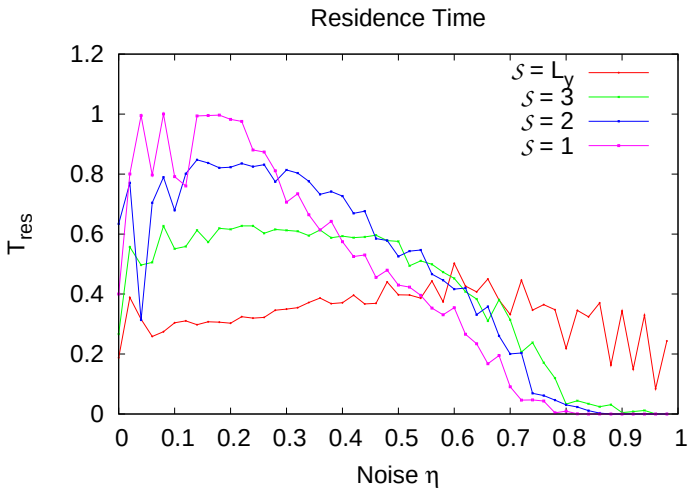

Figure 6.10: Plot of T_{res} against η for different values of $\mathcal{S}$ ($\mathcal{S} = L_y$, $\mathcal{S} = 3$, $\mathcal{S} = 2$, $\mathcal{S} = 1$). To notice that, for enough low noises, as smaller is $\mathcal{S}$ as longer the particles are stopped close to the bottleneck.

For too low values of the noise the values of T_{res} are very high because the particles are forced to follow each-other. On the contrary, for very big values of the noise the particles perform random walks, hence no queue comes up. It is worth to notice that, as expected, lower values of the gap $\mathcal{S}$ involve higher probability to find the particles blocked very close to the maximum constrain. This result makes a point of the importance of the suitable geometrical and environmental condition in order to reach as fast as possible, for instance, a region particularly rich of food.

For these reasons, one could simulate the presence of food within the system and study which is the best geometrical configuration that helps the self-propelled units (bacteria in this case) to reach the food.
In fig. 6.11 I report a sequence of frames of a rectangular system with a constrain in the middle and $N = 1000$ particles initially located on the left. Notice that the food is represented by the box in the right part of the system.

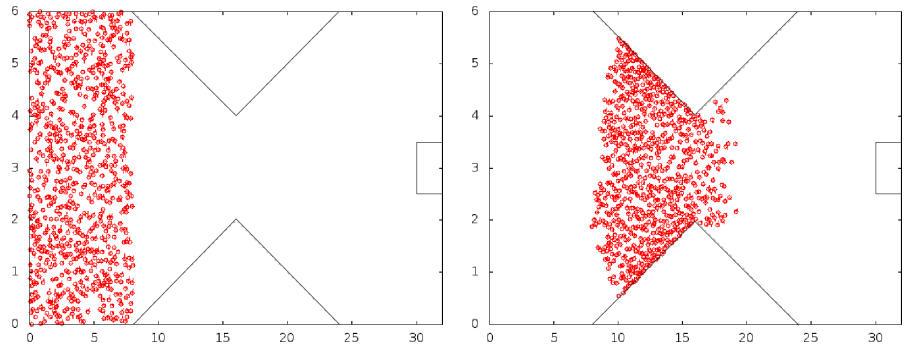

(a) t=0 (b) t=126

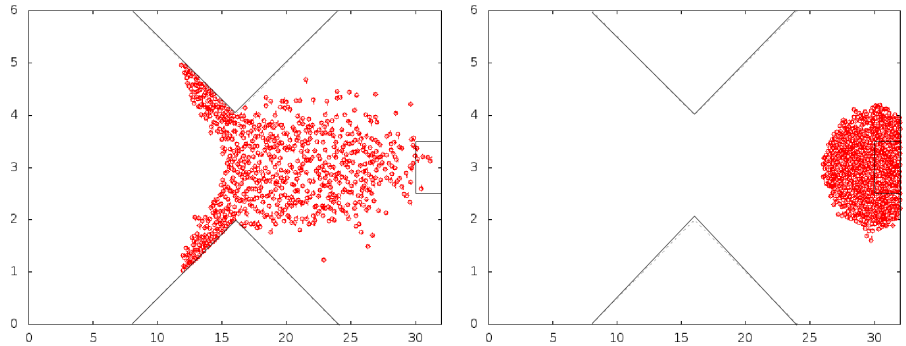

(c) t=284 (d) t=500

Figure 6.11: Snapshots of the system configuration at different step time.

One of the observables which is reasonable to investigate could be the "First Arrival Time" $T_{fat}(t, \eta, \alpha, w)$; or, in other words, the probability that a particle reaches the box as a function of the time t, the noise and the geometry. In this thesis I am not going to investigate further these kind of systems.

From these preliminary considerations, another interesting question arises: What happens if we consider systems without spatial symmetry? Or at least, one of the two part of the system (right or left) is not the mirror of the other? This question is strongly related to the work of Prof. Ruocco [36] and of Prof. Austin [12] which are obtaining solid results based on the possibility for the active matter to overcome the restrictions imposed by the second law of thermodynamics on equilibrium passive systems.
In order to investigate this topic we could remove one part of the constrain and create a sort of funnel, very similar but not equal to that produced by [12]. The most curious thing is that, from a biological point of view, we are just reproducing the same geometry of the valves inside the human veins. As a consequence, we expect that the self-propelled units experience the

same process of the blood cells inside the human veins, i.e. they are forced to flow on the right way. The system we set looks like fig. 6.12.

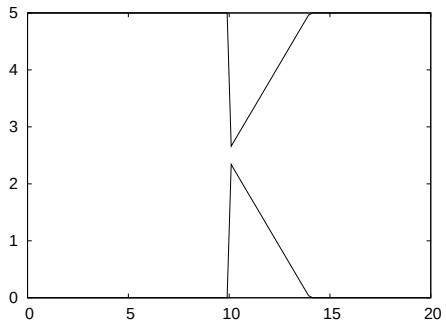

Figure 6.12: Asymmetric constrain.

While fig. 6.13 is a snapshot of the system made of $N = 1000$ particles moving through the constrain.

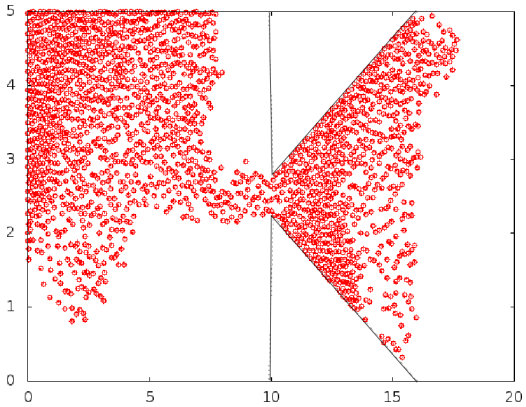

Figure 6.13: Snapshot of a system with $N = 1000$ particles and asymmetric bottleneck. Notice the focusing effect caused by the constrain.

In fig. 6.13 one can notice that under the appropriate environmental and geometrical conditions, the cluster conserve the shape of the constrain, instead of immediately spread. We can define this tendency of the clusters to conserve the shape and the alignment as a "focusing effect".
An important consequence of this feature is, as we will see better later, the enhancing of the cluster average velocity. Since the particles are forced by the interaction with the walls to stay very close and to reduce the fluctuations, the velocity of the cluster center of mass increases. What would be very worthy to investigate further is how much we can focus the clusters. Or in other words, how much the geometry can help the cluster to reach

rapidly a fixed region. As in the case of the chemotaxis term, we are not going to study deeper this scenario.

6.2.2 Focusing Effect

In previous section we have qualitatively observe a tendency of the cluster to stay aligned and to conserve the elongated shape. This feature is very similar to the focusing experienced by the light when pass through a lens. For this reason we called it "focusing effect". In this section we are going to study deeper the occurrence of non homogeneous density patterns in proximity of the narrowest region at the bottleneck. We will investigate in particular the full 2D density distribution function and the local order parameter, which we will define later.

2D Density Distribution

Let us define the two dimensional density distribution $\rho(x, y)$ as

$$\rho(x, y) = \frac{1}{N} \langle \sum_{i=1}^{N} \delta[x\hat{x} + y\hat{y} - \boldsymbol{r}_i] \rangle \tag{6.6}$$

where $\langle \dots \rangle$ is the average over the configurations.
Fig. 6.14 show a sequence of different $\rho(x, y)$ for systems with $N = 1000$ particles and different values of $\mathcal{S}$ and η.
In these figures is clearly visible a strong non uniformity of the density distribution. In particular, it is evident that for the suitable combination of η and $\mathcal{S}$ the darker (denser) region takes an elongated shape. This means that, when the system have broken the initial symmetry for x-axis reflection at $L_x/2$ one side of the bottleneck thrusts out the focused clusters, while the other works as a funnel. In fig. 6.14e and 6.14f the gap is very small and the "plaques" of blocked particles are evident. Otherwise, for bigger values of the gap (6.14a,6.14b) the flow is much more important then the blocked particles, also if not very focused.
The best combination of environmental noise and geometrical shape among these cases is plotted in fig. 6.14d. The gap fixed at $\mathcal{S} = 2$ and the noise at $\eta = 0.1$ involve a good compromise between flowing and focusing.

Local Order Parameter

At this point a question that arise naturally is: which is the best observable we can define in order to investigate a large number of $\mathcal{S}$ and η combinations? One can indeed notice that as soon as the cluster leaves behind the

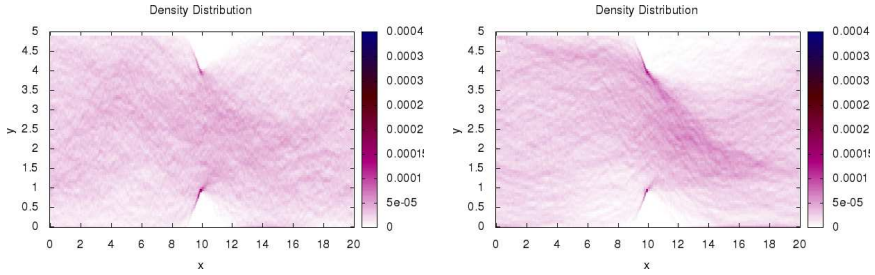

(a) $\mathcal{S} = 3$, $\eta = 0.2$

(b) $\mathcal{S} = 3$, $\eta = 0.1$

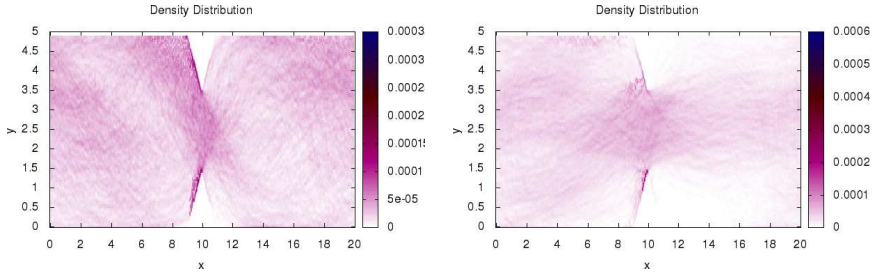

(c) $\mathcal{S} = 2$, $\eta = 0.2$

(d) $\mathcal{S} = 2$, $\eta = 0.1$

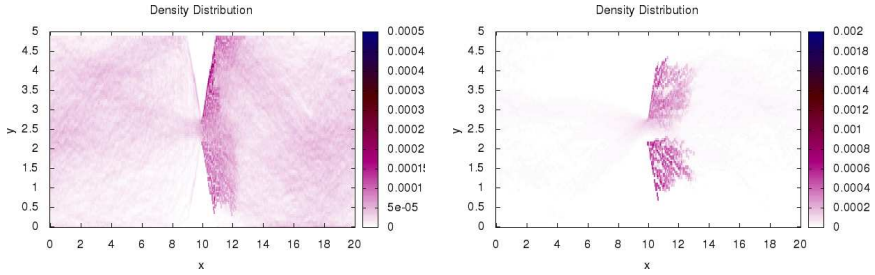

(e) $\mathcal{S} = 0.5$, $\eta = 0.2$

(f) $\mathcal{S} = 0.5$, $\eta = 0.1$

Figure 6.14: Notice (specially for 6.14c and 6.14d) the color scale at the right of the figures. In fig 6.14e the particles are blocked and the flow through the gap is very poor. Notice, also, that the breaking of the symmetry could be rightward or leftward. In the last two figures is leftward, in the others is rightward. Since the system is symmetric for refection of the x-axis around $L_x/2$ the two possibilities have the same probability.

gap it is very coherent, or in other words, the particles are very aligned. Hence the average velocity of that cluster is expected to be bigger than that of a cluster in the original Vicsek model at the same value of the noise, and this effect is more evident as the noise increases. Thus, a good way to check the efficiency of the constrain is to define the local order parameter:

$$\phi_{Loc}(x) \equiv \langle \frac{1}{Nv_0} \left| \sum_i^{\mathcal{C}} \boldsymbol{v}_i(t) \right| \rangle \tag{6.7}$$

where $\langle \dots \rangle$ is the average over the time and the sum is restricted to those particles inside the layer $[x, x+dx]$, or in other words $\mathcal{C} = \{i | \boldsymbol{x}_i \hat{x} \in [L_x/2 - w, L_x/2 + w]\}$. And in the same way we can define the local order parameter fluctuations $\chi_{Loc}(x) = \mathrm{Var}(\phi_{Loc}(x))$.
The figures 6.15a and 6.15b show the trends of $\phi_{Loc}(x)$ and $\chi_{Loc}(x)$ against the x value. Notice that the maximum constrain is set in $x = L_x/2 = 5$.

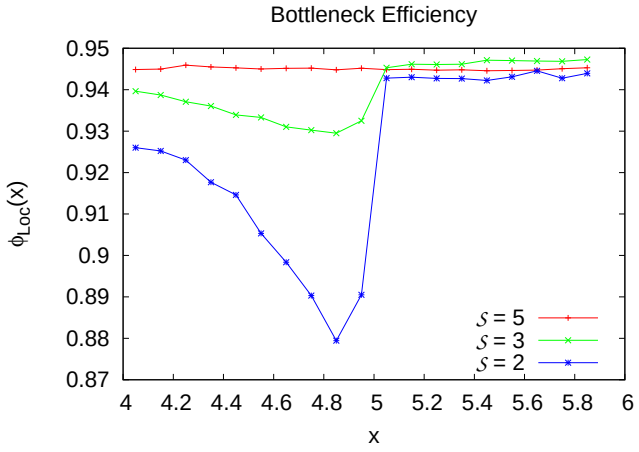

(a)

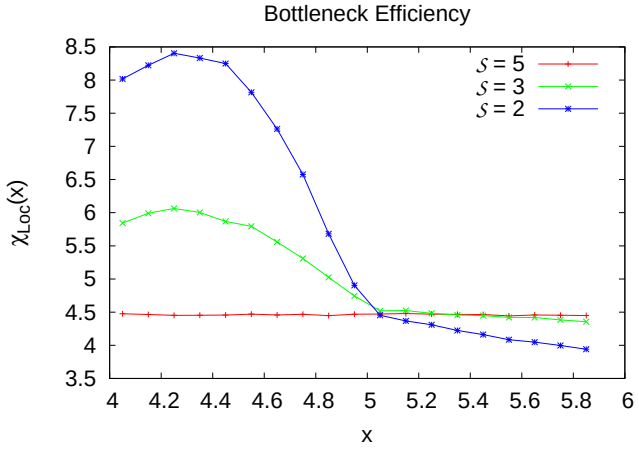

(b)

Figure 6.15: Plot of the local order parameter $\phi_{Loc}(x)$ and $\chi_{Loc}(x)$ as a function of the x value close to the maximum constrain for different values of $\mathcal{S}$ ($\mathcal{S} = L_y$, $\mathcal{S} = 3$ and $\mathcal{S} = 2$) and for fixed value of the noise $\eta = 0.2$.

The focusing effect is visible but not very accentuated in fig. 6.15a and 6.15b because the order parameter value of the "pure" Vicsek case is already very

high. Otherwise when the noise is fixed to $\eta = 0.8$ the increasing of the order parameter close to the constrain is clearly evident, although once the particles have left the bottleneck the noise overwhelms the alignment effect (fig. 6.16a and 6.16b).
These clues strongly suggest a deeper study of the bottleneck efficiency as a function of the environmental noise and the geometrical shape of the constrain.

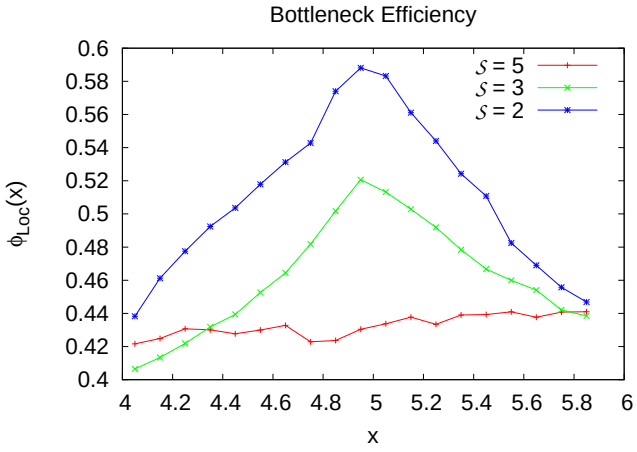

(a)

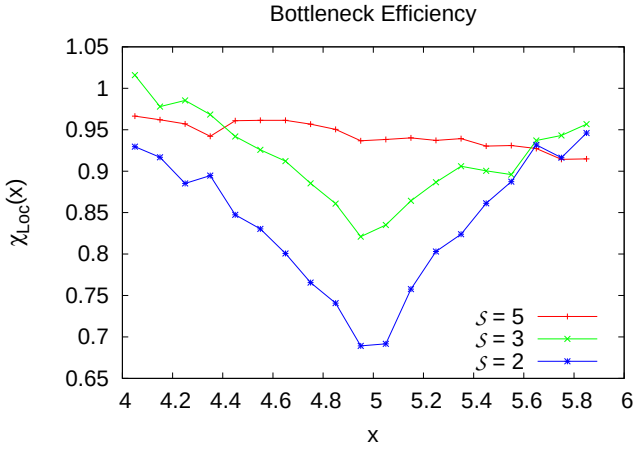

(b)

Figure 6.16: Plot of the local order parameter $\phi_{Loc}(x)$ and $\chi_{Loc}(x)$ as a function of the x value close to the maximum constrain for different values of $\mathcal{S}$ ($\mathcal{S} = L_y$, $\mathcal{S} = 3$ and $\mathcal{S} = 2$) and for fixed value of the noise $\eta = 0.8$.

6.2.3 Spatial Correlation

In this last section we would like to offer an other clue about what is the contribution brought by the passage through the constrain in the cluster shape and density. Since that we are going to use the "spatial correlation" defined in previous chapters the following results have to be compared to sec. 3.2. We expect an important increasing of the clusters density in the case of confining geometries. The sequence reported below (fig. 6.17a-6.17d) shows indeed clearly (notice the scales at the right of each plot) that the narrower is the bottleneck the denser are the clusters.

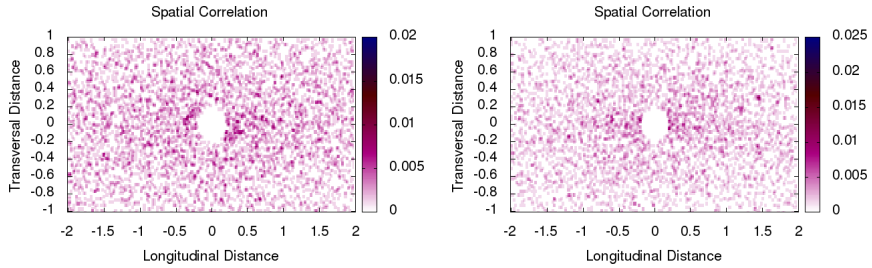

(a) $\mathcal{S} = L_y$ (b) $\mathcal{S} = 3$

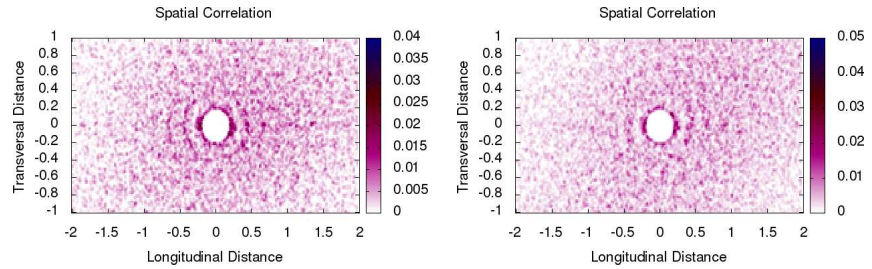

(c) $\mathcal{S} = 1$ (d) $\mathcal{S} = 0.5$

Figure 6.17: Spatial Correlation for different systems with different minimum space between the walls of the constrain. **Notice carefully the scales at the right of the plots**.

We could also study the "orientation correlation" $h(x, y)$ which is the probability of each particle with direction θ to have a neighbour with $\theta_n \in [\theta - d\theta, \theta + d\theta]$ in the region $\mathcal{A} = [x, x + dx][y, y + dy]$. This observable could be very useful to understand if the clusters which were passed through the constrain are more aligned then the cluster which were not gone through. And so if their average velocity is greater of that one of those clusters which not pass through the gap. But, since that we have already found apt observables ($\phi_{Loc}(x)$ and $\chi_{Loc}(x)$) for this purpose, we skip this effort and move later this check if it will be necessary for our aims.

7 Conclusions

In this thesis we have studied numerically the non-equilibrium properties of 2D systems of self-propelled particles (active systems) under geometrical constraints. After having reviewed the classical Vicsek model in the bulk (chap. 2) we introduced a new model that is still based on Vicsek's interaction and updating rules but with the addition of excluded volume interaction between particles. This new model is simulated and compared with the classical Vicsek's model in the bulk (chap. 3). The main result we found is that presence of self-avoidance increases the tendency of the system to stay in the ordered phase. This tendency is quantified by the shift of the order-disorder transition towards higher values of noise and by the narrowing of the order parameter fluctuations. Both effects become more relevant for higher values of the system density. This agrees with the idea that, for instance, denser bacterial systems are more inclined to stay ordered. We next turned to the main argument of the thesis, namely the study of active systems under confinement (chap. 4). This has been carried out by looking first at regular geometries such 2D channels (stripes). We found that if bouncing-back conditions are considered at the stripe boundaries, the system is more inclined to form big clusters than in the unconstrained case. Moreover the giant fluctuations, that are characteristic of active systems in the bulk, are shown to develop also in the confined case and are actually enhanced by making the stripes narrower (sec. 4.3). To better reproduce the behaviour of real bacterial systems close to an impenetrable boundary we then replace the bouncing-back with slip conditions. By inserting this condition in our Vicsek's model with self-avoidance we have been able to recreate adhesion and trapping effects experimentally observed in systems made of more complicated self-propelled rods. For example trapping is studied in details in

chap. 6, where regular stripes are replaced by wedges and bottlenecks. We indeed pointed out the fact that, even at high values of the noise and even without the presence of a chemotaxis term (food), it exists a proper aspect ratio of the wedge that allow to cage a certain fraction of particles within it and keep them for quite long time. Bottlenecks were studied by introducing new observables, as the full 2D density distribution function $\rho(x, y)$ and the local order parameter $\phi(x)$. The most relevant achievements regarding this topic are the occurrences, under suitable conditions, of "blockage" and "focusing" effects. We indeed studied how the geometrical and environmental conditions affect the behaviour of active round particles near the narrowest opening. We found an interesting persistence of the cluster to keep the shape and the coherence of the motion obtained after the passage through the opening. This is a very remarkable feature and it is worthy of deeper investigations.
Asymmetric constrains and addition of chemotaxis term are also briefly mentioned in the same chapter.

As we mentioned in the introduction, technology improvements allow us to reproduce experimentally confined active systems at micro and nano scales. For instance, the researchers of Sheffield University built asymmetric balls by coating half of them in platinum which react with the environment filled of hydrogen peroxide and water. In this way the researchers make microballs self-propelled for the time enough to be observed. As one can read from their website: "our efforts move toward self-propelled nano-swimmers that could navigate narrow channels such as the human circulatory system"[†].
One of the greatest difficulties related to this experiment and, in general, to designing models of active systems is the presence of hydrodynamic interactions among the self-propelled units. Since most part of real active systems live in solutions, hydrodynamics effects play a major role in governing the overall dynamics of the problem. At the state of the art, the implementation of the hydrodynamic is in general a quite difficult task to achieve, even for passive systems. This is one of the reason why first attempts to understand theoretically active systems referred to cases, as the one described in [9], in which hydrodynamic modes are .

With respect to these comments, other questions could be addressed: How can we include hydrodynamic interaction in the original Vicsek model? How is it possible to design a model able to describe the recursive patterns (vortexes, rings, bands, ...) shown by active particles in aqueous bath?
Even excluding hydrodynamic, other kind of questions are still present; for instance how can we describe and predict theoretically the confinement effects on order-disorder transition?

[†] www.sheffield.ac.uk/physics/stories/microswimmer

In order to seek for some solutions, it could be interesting to compare our results with a real experiment and develop together new models able to reproduce a larger range of features shown by real systems, like the already mentioned, vortexes and rings. These are only some of the questions which naturally arise in this topic. Active matter and its confinement is a very broad and practical topic, full of theoretical challenges which deserve deeper studies.

A
Funnel

Strongly inspired by [12] we endeavoured to reproduce a sort of funnel inside a 2d channel. Quite unexpectedly, the authors report a strongly asymmetric density distribution of the steady state, which confirm the fact that bacteria are *not* random walkers, and that the interaction bacteria-surfaces is very relevant. Here, we try to reproduce the same behaviour using self-propelled round particles interacting through the alignment rule introduced by Vicsek. The set up is made of a rectangular box with slip condition on the four walls and a funnel with the sharpest part leftward. To notice that neither the walls at $x = 0$ and $x = L_x$ have the periodic conditions. Fig. A.1 represent two different configurations of system.

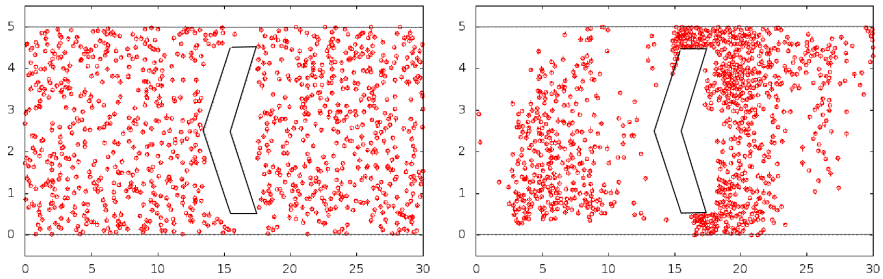

(a) $t = 0$ **(b)** $t = 500$

Figure A.1: Snapshots of system configurations at time t specified below the plots. Notice the increasing of the density in the right part of the box.

One of the most important observables measured in [12] is the density in the right part of the system $\rho(x > L_x/2)$ as a function of the time t. In fig.

A.2 we report the results from our simulations which agree with the results of Prof. Austin. The plot shows the density in the right part of the system as a function of the time steps. What it is worth to notice is the increasing of the density from an initial value of $\rho \simeq 1/2$, which means uniform density inside the box, to a final value $\rho(x > L_x/2) = 0.8$ which means that the most part of the particles is in the right half of the system.

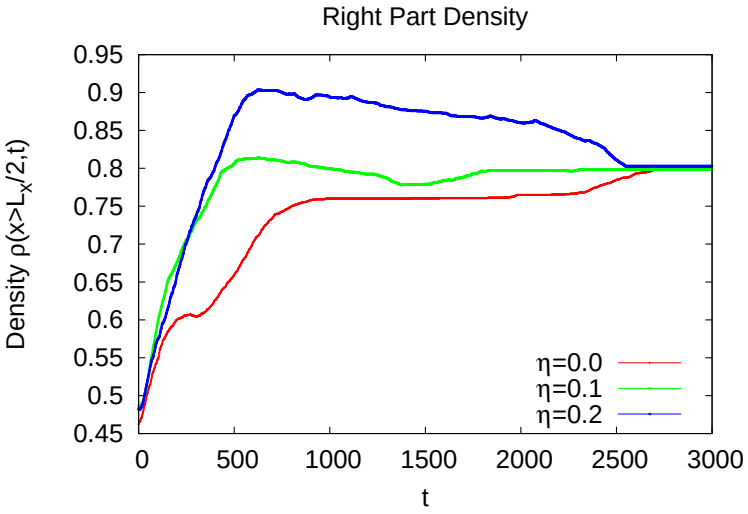

Figure A.2: Plot of the density in the right part of the system as a function of the time and for different values of the noise. To notice that, against the Gibbs law, the density increases, instead of stay constant. The simulation is averaged over 10 different initial conditions.

It is also worth to notice that different values of the noise imply different behaviours of $\rho(x > L_X/2, t)$ before it reaches the steady state. It could be interesting comparing numerical data with the experimental ones in order to find the most suitable value of the noise η which can reproduce the real bacteria behaviour. As a consequence one can find out the noise experienced by a real bacterial system.

This brief review on the experiment of Prof. Austin [12] makes a point of the relevance of the bacteria-surface interaction. Active systems often show non-intuitive scenarios and spectacular behaviours when interacting with obstacles and irregular walls. For these reasons confinement, trapping and mazes could turn out useful and powerful tools in order to handle this kind of systems and deserve deeper studies.

Bibliography

[1] J.K. Perrish, E.-K. Leah *Complexity, pattern and evolutionary trade-offs in animal aggregation*, Science **284**, 99-101 (1999)

[2] Becco et al. *Experimental evidences of a structural and dynamical transition in fish school*, Physica A **367**, 487-493 (2006)

[3] W.K. Potts *The chorus line hypothesis of maneuver coordination in avian flocks*, Nature **309**,344-345 (1984)

[4] O. Petit and R. Bon *Decision-making processes: the case of collective movements*, Behav Processes **84(3)**,635-47 (2010)

[5] J.A. Shapiro, M. Dworkin *Bacteria as multicellular organisms*, Oxford University Press 1997

[6] P. Friedl *Prespecification and plasticity: shifting mechanisms of cell migration*, Current Opinion in Cell Biology **14(1)**, 14-23 (2004)

[7] T.S. Deisboeck, I.D. Couzin *Collective behavior in cancer cell populations*, Bioessays **31(2)**, 190-197 (2009)

[8] S. Ramaswamy *The Mechanics and Statistics of Active Matter*, Ann.Rev.Cond.Mat.Phys. **1**, 323-345 (2010)

[9] J. Deseigne, O. Dauchot, and H. Chaté *Collective Motion of Vibrated Polar Disks* Phys. Rev. Lett. **105**, 098001

[10] T. Vicsek, A. Czirok, E. Ben-Jacob, I. Cohen, O. Shochet *Novel type of phase transition in a system of self-driven particles*, Phys.Rev.Lett. **75**, 6 (1995)

[11] T. Vicsek *Collective Motion*, arXiv:1010.5017v1

[12] P. Galajda, J. Keymer, P. Chaikin, R. Austin *A Wall of Funnels Concentrates Swimming Bacteria* Journal of Bacteriology **189**, 23 (2007)

[13] G. Grégoire, H. Chaté *Onset of collective and cohesive motion*, Phys. Rev. Lett. **92**, 025702 (2004)

[14] H.P. Zhang, A. Be'er, E.-L. Florin, H.L. Swinney *Collective motion and density fluctuations in bacterial colonies*, PNAS **107**, 31 (2010)

[15] G. Baglietto, E.V. Albano *Nature of the order-disorder transition in the Vicsek model for the collective motion of self-propelled particles*, Physical Review E **80**, 050103(R) (2009)

[16] J. Toner, Y. Tu *Flocks, herds, and schools: A quantitative theory of flocking*, arχiv:cond-mat/9804180v1 (1998)

[17] J. Toner, Y. Tu *How birds fly together: Long-range order in a two-dimensional dynamical XY model*, arχiv:adap-org/9506001v1 (1995)

[18] J.A. Pimentel, M. Aldana, C. Huepe, H. Larralde *Intrinsic and extrinsic noise effects on the phase transition of swarming systems and related network models*, arχiv:0802.3879v1

[19] A.A. Chepizhko, V.L. Kulinskii *On the relation between Vicsek and Kuramoto models of spontaneous synchronization*, arχiv:1005.2140v3

[20] T. Vicsek, H.E. Stanley, A. Czirok *Spontaneously ordered motion of self-propelled particles*, J. Phys. A: Math. Gen. **30**, 1375 (1997)

[21] H. Chaté, F. Ginelli, G. Grégoire, F. Raynaud *Collective motion of self-propelled particles interacting without cohesion*, Phys. Rev. E **77**, 046113 (arχiv:0712.2062v1)

[22] G. Baglietto, E. Albano *Computer simulation of the collective displacement of self-driven individuals*, Computer Physics Communications **180**, 527-531 (2009)

[23] G. Baglietto, E. Albano, *Finite-size scaling analysis and dynamic study of the critical behavior of a model for the collective displacement of self-driven individuals*, Phys. Rev. E **78**, 021125 (2008)

[24] V. Dossetti, F.J. Sevilla, V.M. Kenkre *Phase transitions induced by complex nonlinear noise in a system of self-propelled agents*, arχiv:0806.0882v3

[25] M. Nagy, B. Gonci, T. Vicsek *Phase transition in the scalar noise model of collective motion in three dimensions*, arχiv:0801.0151v2

[26] M. Nagy, I. Daruka, T. Vicsek *New aspects of the continuous phase transition in the scalar noise model (SNM) of collective motion*, arχiv:nlin/0611031v1

[27] A. Czirok, A.L. Barabasi, T. Vicsek *Collective motion of self-propelled particles: kinetic phase transition in one dimension*, Phys. Rev. Lett. **82**, 209-212 (1999)

[28] H. Chaté, F. Ginelli, R. Montagne *Simple Model for Active Nematics: Quasi-Long-Range Order and Giant Fluctuations*, Phys. Rev. Lett. 96, 180602

[29] E. Orlandini, G. P. Saracco, G. Gonnella, D. Marenduzzo *Shearing self-propelled suspensions: arrest of coarsening and suppression of giant density fluctuations*,

[30] F. Peruani, L. Schimansky-Geiger, M. Bär *Cluster dynamics and cluster size distributions in systems of self-propelled particles*, Eur. Phys. J. Special Topics **191**, 173-185 (2010)

[31] N. D. Mermin, H. Wagner. Phys. Rev. Lett. **17**, 1133 (1966)

[32] F. Peruani, M. Bär, A. Deutsch *Non-equilibrium clustering of self-propelled rods*, Phys. Rev. E **74**, 030904(R) (2006)

[33] J. Elgeti, G. Gompper *Self-propelled rods near surfaces* EPL, **85** (2009)

[34] H.H. Wensink, H. Löwen *Aggregation of self-propelled rods near confining walls*, Phys.Rev. E **78**, 031409 (2008)

[35] A. Kudrolli, G. Lumay, D. Volfson and L. S. Tsimring *Swarming and Swirling in Self-Propelled Polar Granular Rods*, Phys. Rev. Lett. **100**, 058001 (2008)

[36] R. Di Leonardo, L. Angelani, G. Ruocco, V. Iebba, M.P. Conte, S. Schippa, F. De Angelis, F. Mecarini, E. Di Fabrizio *A bacterial ratchet motor* PNAS **107** (21) 9541-9545 (2010)